

**Assessment of Active State Titin's Effects on Muscle  
Mechanics Using Finite Element Modeling**

by

**Alican Onur ankaya**

B.Sc., Mechactronics Engineering, Baheşehir University, 2014

Submitted to the Institute of Biomedical Engineering  
in partial fulfillment of the requirements  
for the degree of  
Doctor  
of  
Philosophy

Boğaziçi University

2022

## ACKNOWLEDGMENTS

I would like to acknowledge my advisor Prof. Can A. Yücesoy. He was an admirable example of a mentor. His persistence in introducing the ways of an academic and his guidance helped me to complete this thesis.

Besides my advisor, I'd like to acknowledge my committee members: Prof. Burak Güçlü, Prof. Yunus Ziya Arslan, Prof. Kiisa Nishikawa and Prof. Oliver Röhrle for their insights on my work.

Honored to be a part of Biomechanics Lab. My lab colleagues Evrim, Uluç, and Cemre Su, I wish them the best. Their hard work motivated me to do better.

Also, cheers to my friends Esra, Doğan, İlayda, and Serap. They filled this journey with joyful memories. I'm glad that it was in the universe's plans for our paths to crossed in this institute.

I deeply thank my father and mother. I simply would not be able to take up this challenge without their love and support. This goes not only for supporting my PhD, but also for my whole life. I deeply appreciate their generosity, love, and patience.

I would like to thank Serap and Şenay. The Way was lit, the Path was clear, and I required only the Strength to follow it. With your presence the Light gained purchase, you lifted my Spirit, and you made the Purpose clear. Thank you for giving me the strength to getting through and finish this.

Lastly, my sincere gratitude to my dear friend Serap. This journey was excruciating for one to walk alone, and I simply would not have achieved without your companionship. May our friendship transcend through life.

## ACADEMIC ETHICS AND INTEGRITY STATEMENT

I, Alican Onur Çankaya, hereby certify that I am aware of the Academic Ethics and Integrity Policy issued by the Council of Higher Education (YÖK) and I fully acknowledge all the consequences due to its violation by plagiarism or any other way.

Name :

---

Signature:

---

Date:

---

## ABSTRACT

### Assessment of Active State Titin's Effects on Muscle Mechanics Using Finite Element Modeling

Calcium dependent mechanical behaviors characterize titin's contribution to force production in three-myofilament paradigm: (1) Stiffening of PEVK (Proline, Glutamate, Valine, Lysine) segment, and (2) reduction of free-spring length via N2A-titin binding. This thesis is focused on the introduction of an alternative perspective to the analysis of titin with incorporating epimuscular myofascial loads. Isolated and integrated rat muscle finite element model variations were used with three titin models: passive state titin, active state titin-I and active state titin-II. Results of isolated model showed that active state titin-I and II limits sarcomere shortening ( $l_m = 32.7\text{mm}$ : up to 10% and 20%, respectively). Such shorter sarcomere effect characterizes active state titin's mechanism of effects. Integrated models showed that the shorter sarcomere effect becomes an inconsistent and variable mechanism: Shorter sarcomere effect is further enhanced for proximal fascicle interfaces (by 30.2% and 31.0%, respectively) whereas it is also diminished for remaining fascicles (by 10.3% and 14.0%, respectively), but even a longer sarcomere effect is shown. Overall, titin's mechanism of effect and functionality are manipulated by epimuscular myofascial force transmission. This implies a new approach for the 3-myofilament model: For the analysis of the components of the contractile machinery, contribution to force production and contribution to muscle mechanics should be assessed with alternative perspectives. Titin's calcium dependent mechanical behaviors belong to former as these increases its stiffness, whereas shorter sarcomere effect belongs to latter as this mechanism further translates its effect to other components as well as to length-force characteristics. These together comprehensively define titin's contribution as a third myofilament.

**Keywords:** Force Enhancement, Titin, Shorter Sarcomere Effect, Epimuscular Myofascial Force Transmission, Epimuscular Myofascial Loads, Finite Element Modeling

## ÖZET

### Aktif Koşul Titin'in Kas Mekanikleri Üzerindeki Etkisinin Sonlu Elemanlar Modellemesi ile İncelenmesi

Kalsiyum bağlantılı mekaniksel davranışları titinin üç-miyofilaman paradigması dahilinde kuvvet üretimini karakterize etmektedir: (1) PEVK (Prolin, Glutamat, Valin, Lizin) segmentinin sertleşmesi ve (2) N2A-titin etkileşimi ile serbest yay uzunluğunun kısalması. Bu tez, titinin epimüsküler yüklerin dahil edildiği alternatif bir perspektifle analizlerine odaklanmaktadır. İzole ve entegre sıçan sonlu elemanlar kas model varyasyonları üç farklı titin modeli ile birlikte kullanılmıştır: pasif koşul titin, aktif koşul titin-I ve aktif koşul titin-II. İzole kas modeli sonuçları aktif koşul titin-I ve titin-II'nin sarkomer uzamasını sınırladığını ( $l_m = 32.7\text{mm}$ : sırasıyla %10'a ve %20'ye kadar) göstermiştir. Bu kısa sarkomer etkisi aktif koşul titinin etki mekanizmasıdır. Entegre kas modelleri sonuçları kısa sarkomer etkisinin dengesiz ve bağımlı bir değişken haline geldiğini göstermektedir: kısa sarkomer etkisi proksimal fasiküller için gelişmiş (sırasıyla %30.2 ve %31.0), kalan fasiküller için ise azalmıştır (sırasıyla %10.3 ve %14.0) ve uzun sarkomer etkisi görülmüştür. Titinin etki mekanizması ve fonksiyonel etkileri epimüsküler miyobağdoku kuvvet iletimi tarafından manipüle edilmiştir. Bu bulgular 3-miyofilaman modeli için yeni bir yaklaşım ifade eder: Kontraktıl modeli komponentlerinin analizlerinde kuvvet artışına katkısı ve kas mekaniklerine katkısı farklı perspektifler ile ele alınmalıdır. Titinin kalsiyum bağlantılı mekaniksel davranışları titinin sertliğini arttırdığı için ilkinde dahildir. Öte yandan, kısa sarkomer etkisi ise titinin etkisini diğer komponentlere ve kuvvet-uzunluk karakteristiklerine ilettiği için ikincisine dahildir. Bu özellikler titinin üçüncü miyofilaman olarak katkısını kapsamlı olarak tanımlamaktadır.

**Anahtar Sözcükler:** Kuvvet Artışı, Titin, Kısa Sarkomer Etkisi, Epimüsküler Miyobağdoku Kuvvet İletimi, Epimüsküler Yükler, Sonlu Elemanlar Modeli.

## TABLE OF CONTENTS

ACKNOWLEDGMENTS . . . . .	iii
ACADEMIC ETHICS AND INTEGRITY STATEMENT . . . . .	iv
ABSTRACT . . . . .	v
ÖZET . . . . .	vi
LIST OF FIGURES . . . . .	x
LIST OF TABLES . . . . .	xii
LIST OF SYMBOLS . . . . .	xiii
LIST OF ABBREVIATIONS . . . . .	xiv
1. INTRODUCTION . . . . .	1
1.1 Two-Myofilament Model . . . . .	1
1.2 Titin Structure . . . . .	1
1.3 Titin's Role in Passive and Active Muscle Mechanics . . . . .	2
1.3.1 Elastic recoil and elastic energy storage . . . . .	3
1.3.2 Ig domain unfolding/refolding . . . . .	3
1.3.3 Calcium dependent stiffening . . . . .	3
1.4 Scope of Titin Literature . . . . .	4
1.5 Epimuscular Myofascial Force Transmission (EMFT): Connective tissue and associated forces . . . . .	5
1.6 Motivation of the thesis . . . . .	6
1.7 Overview of thesis . . . . .	7
2. The effects of an activation-dependent increase in titin stiffness on whole muscle properties using finite element modeling . . . . .	9
2.1 Introduction . . . . .	9
2.2 Methods . . . . .	10
2.2.1 Isolated EDL Model . . . . .	11
2.2.2 Passive and active state titin cases . . . . .	12
2.2.3 Solution procedure . . . . .	13
2.2.4 Processing of data . . . . .	13
2.3 Results . . . . .	14

2.4	Discussion . . . . .	18
3.	Principles of the Mechanism for Epimuscular Myofascial Loads Leading to Non-uniform Strain Distributions Along Muscle Fiber Direction: Finite Element Modeling . . . . .	23
3.1	Introduction . . . . .	23
3.2	Materials and Methods . . . . .	25
3.2.1	Description of the "Linked Fiber-Matrix Mesh Model" . . . . .	25
3.2.2	LFMM Model Features and Definitions . . . . .	26
3.2.3	Muscle Models Studied . . . . .	26
3.2.4	Cases Studied . . . . .	29
3.2.5	Solution Procedure . . . . .	31
3.2.6	Processing of Data . . . . .	31
3.3	Results . . . . .	32
3.3.1	Case I: Passive Isometric Muscle, With Imposed Relative Position Changes . . . . .	32
3.3.2	Case II: Passive Lengthened Muscle . . . . .	32
3.3.3	Case III: Active Isometric Muscle, With Imposed Relative Position Changes . . . . .	34
3.4	Discussion . . . . .	36
3.5	CONCLUSION . . . . .	41
4.	Titin EMFT Article . . . . .	42
4.1	Introduction . . . . .	42
4.2	Methods . . . . .	43
4.2.1	Isolated EDL Model . . . . .	44
4.2.2	Extramuscularly Connected Model . . . . .	45
4.2.3	Epimuscularly connected muscle . . . . .	46
4.2.4	Passive and active state titin cases . . . . .	46
4.2.5	Solution procedure . . . . .	48
4.2.6	Processing of data . . . . .	48
4.3	Results . . . . .	49
4.3.1	Local effects of EMFT, manipulating effects of active state titin . . . . .	49

4.3.2	Global effects of EMFT, manipulating functional effects of active state titin . . . . .	53
4.4	Discussion . . . . .	55
5.	General Discussion . . . . .	60
5.1	An alternative perspective for the Third Myofilament . . . . .	60
5.2	An alternative perspective for the Three-Myofilament Model . . . . .	60
APPENDIX A.	APPENDIX A: LINKED FIBER MESH MATRIX MODEL . . . . .	62
A.1	Isolated EDL muscle model . . . . .	62
A.1.1	ECM element . . . . .	63
A.1.2	Myofiber element . . . . .	64
A.1.3	Linking elements . . . . .	66
A.1.4	Aponeurosis element . . . . .	66
REFERENCES	. . . . .	68

## LIST OF FIGURES

Figure 1.1	Sarcomere structure	2
Figure 2.1	Finite element model of EDL muscle of the rat.	11
Figure 2.2	The stress-strain characteristics of titin in the reference model (passive state titin) and extended models (active state titin-I and active state titin-II).	13
Figure 2.3	The force-length characteristics of the modeled EDL muscles in the range of muscle lengths studied).	15
Figure 2.4	Mean nodal fiber direction strain and stresses at $l_m = 32.7\text{mm}$ per fascicle interface.	16
Figure 2.5	Mean nodal fiber direction strain and stresses at $l_m = 32.7\text{mm}$ per fascicle interface.	17
Figure 3.1	Finite element model of EDL muscle of the rat.	25
Figure 3.2	Anatomy and geometry of the model cases studied.	28
Figure 3.3	Schematic representation of the protocols modeled.	30
Figure 3.4	Results presented for Case I: Passive isometric muscle, with imposed relative position changes.	33
Figure 3.5	Results presented for Case II: Passive lengthened muscle.	35
Figure 3.6	Results presented for Case III: Active isometric muscle, with imposed relative position changes.	37
Figure 4.1	Finite element model of EDL muscle of the rat.	44
Figure 4.2	Anatomy and geometry of the model cases studied.	47
Figure 4.3	Nodal fiber direction strains for distal fascicle sections (III-IV) at $l_m = 32.7\text{mm}$ per fascicle interface	50
Figure 4.4	Nodal fiber direction strains for proximal fascicle sections (I-II) at $l_m = 32.7\text{mm}$ per fascicle interface.	51
Figure 4.5	Mean nodal fiber direction strain and stresses for active state titin-I at $l_m = 32.7\text{mm}$ per fascicle interface.	53
Figure 4.6	Mean nodal fiber direction strain and stresses for active state titin-II at $l_m = 32.7\text{mm}$ per fascicle interface.	54

Figure 4.7	The force-length characteristics of the modeled EDL muscles in the range of muscle lengths studied from initial length i.e., $l_m = 28.7\text{mm}$ to $l_m = 32.7\text{mm}$ .	55
Figure A.1	Finite element model of EDL muscle of the rat.	63
Figure A.2	LFMM model concept and plots of constitutive equations defining the muscle modeled.	65

## LIST OF TABLES

Table A.1	Values and definitions of the model constants.	67
-----------	--	----

## LIST OF SYMBOLS

$l_m$	Muscle Length
$l_{m0}$	Optimum Muscle Length
$\varepsilon_{22}$	Mean nodal fiber direction mean strain
$\sigma_{22\text{titin}}$	Mean nodal fiber direction titin stress
$\sigma_{22\text{contr}}$	Mean nodal fiber direction contractile stress
$\sigma_{22}$	Mean nodal fiber direction total stress

## LIST OF ABBREVIATIONS

PEVK	Proline (P), Glutamate (E), Valine (V), Lysine (K)
MDM	Muscular dystrophy with myositis
SSE	Shorter Sarcomere Effect
EDL	Extensor Digitorum Longus
LFMM	Linked Fiber Mesh Model
ECM	Extracellular Matrix
MFT	myofascial Force Transmission
EMFT	Epimuscular myofascial Force Transmission

# 1. INTRODUCTION

## 1.1 Two-Myofilament Model

Two-myofilament model (or "cross-bridge theory" & "sliding filament theory") is widely accepted in the literature as to represent muscle contraction[1],[2] where active force production is based on the degree of overlap between actin and myosin[3][4]. In this model, the force is produced by the thick filaments (myosin) interacting with thin filaments (actin) through the myosin heads in cycles and pulling thin filaments. Overall, this two-myofilament model is regarded as a valid representation of the muscle contraction behavior, especially isometric and concentric contractions. On the other hand, this model falls also short on several ends[5],[6] such as predicting sarcomere characteristics in eccentric contraction[5] and cases where observed force simply differs from the force predicted by the model i.e., static stiffness[7], residual force enhancement[8],[9], and force depression[10]. The inaccuracies and shortcomings of the two-myofilament model based the motivation to seek for a new contraction paradigm including titin[11], a sarcomeric protein discovered later than the development of sliding filament theory.

## 1.2 Titin Structure

Titin, is a large proteins[12] that spans the half-sarcomere. Titin's N terminus begins at Z-line to C terminus ends at M-line[13],[14], and is considered the backbone of the sarcomere[15]. Titin isoforms differentiated by alternative splicing events have structural differences[12]. nonetheless, general structure of titin in skeletal muscle (Figure1.1)[14]: (A-band) this stiff section is mostly contains immunoglobulin (Ig) and fibronectin repeats, and highly associated with myosin[16]. (I-band) The elastic section is composed of proximal Ig tandem, N2A region, proline glutamate valine lysine (PEVK) segment, and distal Ig tandem. Proximal Ig tandem elongates at low forces, whereas extention of PEVK segment begins at high forces[17],[18]. Overall, intra cellu-

lar passive tension of the sarcomere has been predominantly attributed to titin[19],[20].

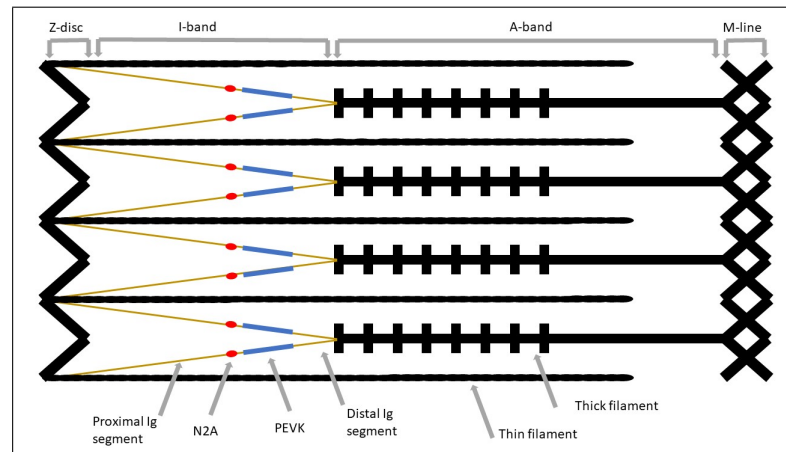


**Figure 1.1** Sarcomere structure including three main components: actin (thin filament), myosin (thick filament), and titin. Titin is further demonstrated as its regions, proximal & distal Ig tandems with PEVK and N2A regions

### 1.3 Titin’s Role in Passive and Active Muscle Mechanics

Titin is ascribed with various roles within the sarcomere, among these roles are signaling, sensing[21],[22], passive tension[23], sarcomere integrity[24], and preserving thick filament’s position within the sarcomere[25] that helps functioning of other filaments.

However, titin’s role is not restricted to those mentioned above. Titin’s involvement in active contraction was proposed recently: It was shown that titin stiffness reaches substantial levels and contributes to force before cross-bridge formation[7], remains for a brief period after muscle fiber is deactivated[26], and can account for the excess force observed in cases like static stiffness[27] and RFE[28]. However, as the connection between these phenomena and titin is established, mechanism of titin regarding these force contributions remains elusive.

Thus, several potential mechanisms potentially explaining titin’s involvement in

active muscle mechanics are proposed[29]:

### **1.3.1 Elastic recoil and elastic energy storage**

Titin's spring-like structure is a basis for titin to react to rapid length changes (e.g., energy storage with stretching & release upon shortening). This elastic recoil was shown in experiments[30], a potential behavior of titin to contribute to muscle dynamics, considering that titin can reach adequate stretch levels within physiological sarcomere ranges[31].

### **1.3.2 Ig domain unfolding/refolding**

Titin's elasticity is mostly due to its highly elastic I-band. Heterogeneous structure of titin cause non-uniform elongation of the I-band: Upon initial stretch, highly elastic Ig tandem segment is primarily elongated whereas PEVK elongation begins at higher levels of stretch[18]. This unfolding/refolding behavior of Ig tandem was further characterized[32], and it was shown that this behavior can occur under physiological stretch levels[33] as titin's response to stretch[29].

### **1.3.3 Calcium dependent stiffening**

Another model developed to explain titin's involvement in active muscle mechanics is the modification of its stiffness in a calcium-dependent manner. It was shown that titin has a calcium affinity[34] and that E-rich motifs in the PEVK segment binds to calcium with high affinity, increasing stiffness of titin[35]. However, this stiffness elevation was not enough to account for excess force observed alone[36], and titin-actin interaction is suggested[37] as an additional calcium-dependent mechanism that further increases the stiffness.

Among these, calcium-dependent stiffness increase is of interest: (1) Both elastic recoil and Ig domain unfolding-refolding mechanisms describe a more complex structure of "passive" spring whereas calcium-dependent behaviors characterize a more "active" behavior. (2) For both elastic recoil and Ig domain unfolding-refolding mechanisms, physiological parameters (e.g., working sarcomere length) needs to be ensured for these mechanisms to function, whereas for the calcium dependent mechanisms, titin "actively" alters its structure to become relevant in the physiological range. (3) Among the calcium-dependent mechanical behaviors, titin binding to actin will potentially render proximal Ig tandem inextensible and affect elastic recoil behavior due to shortened free-spring length, effectively manipulating the other two mechanisms. Titin-actin interaction in skeletal muscle is only studied recently: Responsible Ig parts of N2A segment and associated properties (e.g. calcium concentration dependency, its strength and its stability) are discovered in vitro[38]. Furthermore, titin-based stiffness increase with the role of this mechanism on muscle mechanics were recently shown experimentally[39],[40][41]. These findings reinforced the idea[37] of reduction in titin's free-spring length by titin-actin interaction through N2A region.

## 1.4 Scope of Titin Literature

Studies in general based on protein engineering, myofibril or muscle fiber-based experiments[35],[28],[42]. Such isolated experimental setups enabled analysis of titin exclusively in terms of its structure and mechanism. Recent experiments of whole muscles[39],[40] provided a more complete analysis of titin's role in muscle mechanics. However, potential contribution of connective tissues are excluded in those experiments. Specimens like constituted protein structures or myofibrils are even more isolated as presence of the connective tissue, as well as its effects, is minimal to none[28],[43]. On the other hand, possible effects of connective tissue is minimized in experiments with whole muscles[40]. Hence, the current experiments tend to exclude the connective tissue and focus solely on titin, leading to an incomplete approach in this regard.

## 1.5 Epimuscular Myofascial Force Transmission (EMFT): Connective tissue and associated forces

Main sections of the muscle connective tissue: Tissue layer surrounding the muscle (epimysium), tissue connecting fascicles along the muscle (perimysium), and tissue connecting neighboring muscle fibers (endomysium)[44],[45]. Despite the constituent and structural differences[44],[45], tissue continuity is provided with these tissues[46]. It was shown that these connective tissues are capable of transmitting force, termed as myofascial force transmission (MFT), and the continuity of them is a key aspect of the muscle mechanics: When the connective tissue within the muscle belly is separated, muscle length-force characteristics changes substantially[47].

Muscle in-vivo is not isolated due to external connections such as neuromuscular tract, intraosseous membrane, compartmental fascia and collagenous connections with adjacent muscles[48],[46]. This continuity enables forces to be transmitted to the muscle from surroundings[49][50], presenting an additional pathway for muscles to transmit force besides tendon[51]. Consecutively, this allows forces from surrounding structures, termed as epimuscular myofascial force transmission(EMFT), to affect muscle mechanics: It was shown that these external connections cause proximal-distal force differences[51],[48],[52], as well as changes in force levels and length-force exertion range[53]. Additionally, effects of epimuscular loads on local muscle mechanics are present: Sarcomere length heterogeneity is increased with extramuscular and intermuscular connections[53], both within the same fascicle (serial distribution) and among neighboring fascicles (parallel distribution). This heterogeneity is the characteristic result of epimuscular myofascial loads, which is dependent on muscles in-vivo relative position[54].

## 1.6 Motivation of the thesis

Muscle Force production is associated with the sarcomere lengths that essentially relates to myofilament overlap. Working sarcomere length is also an important criterion for the titin: Its calcium dependent activation behaviors are an effort of titin to "actively" become a relevant component within sarcomere. By increasing its stiffness, titin enhances its response to sarcomere length changes. Any manipulation of sarcomere length will impose a stretch (or compress) on titin, with the resulting effects will be magnified when titin is stiffer. Consecutively, effects that can manipulate sarcomere strain potentially affect effectiveness of titin's calcium-dependent mechanical behaviors. Considering that local strain heterogeneities can be imposed via epimuscular loads, these loads would also have a substantial effect over titin's involvement in contraction mechanics as an active myofilament.

Titin's structure, mechanism, and involvement in muscle mechanics are studied extensively, and potential mechanisms introduced to explain its role. Nonetheless, contribution of the epimuscular myofascial forces are excluded in these analyses, leading to an incomplete approach. A complementary approach in this regard including non-force producing components and epimuscular loads would achieve a whole-muscle context. The linked fiber-matrix mesh model (LFMM) integrates myofascial force transmission along with myotendinous force transmission, and is a suitable muscle model in this regard. Consecutively, this thesis is focused on the introduction of an alternative perspective to the analysis of titin with incorporating epimuscular myofascial loads using finite element modeling. Specific aims in this thesis are:

1. Determine the effect of activation-dependent titin stiffness on contracting skeletal muscle
2. Determining how epimuscular myofascial loads can lead locally to strains opposing those elsewhere within the muscle that are determined by the globally imposed conditions
3. Determining how epimuscular myofascial loads manipulate active state titin ef-

fects

## 1.7 Overview of thesis

Chapter 2 Cankaya A.O., Pamuk U., Yucesoy C.A., 2021. "The effects of an activation-dependent increase in titin stiffness on whole muscle properties using finite element modeling" *Journal of Biomechanics* 116 110197. Aim was to study the mechanism of effects and particularly to determine the functionally more effective active state titin model. Isolated EDL muscle of the rat was modeled and three cases were studied (passive state titin (no change in titin constitutive equation in the active state), active state titin-I (constitutive equation involves a higher stiffness in the active state) and active state titin-II (constitutive equation also involves a strain shift coefficient accounting for titin's reduced free spring length)): Compared to passive state titin, (i) active state titin-I and II elevates muscle total ( $l_m = 32.7\text{mm}$ : 14% and 29%, respectively) and active ( $l_m = 32.7\text{mm}$ : 37.5% and 77.4%, respectively) forces, (ii) active state titin-II also shifts muscle's optimum length to a longer length ( $l_m = 29.6\text{mm}$ ), (iii) active state titin-I and II limits sarcomere shortening ( $l_m = 32.7\text{mm}$ : up to 10% and 20%, respectively). Such shorter sarcomere effect characterizes active state titin's mechanism of effects. These effects become more pronounced and functionally more effective if not only calcium induced stiffening but also a reduced free spring length of titin is accounted for.

Chapter 3 Pamuk U., Cankaya A.O., Yucesoy C.A., 2020. "Principles of the Mechanism for Epimuscular Myofascial Loads Leading to Non-uniform Strain Distributions Along Muscle Fiber Direction: Finite Element Modeling" *Frontiers in Physiology* 11 789. The aim was to test the following hypothesis: epimuscular myofascial loads can lead locally to strains opposing those elsewhere within the muscle that are determined by the globally imposed conditions. Three model variations ((1) isolated muscle and models aiming at representing the principles of a muscle in its in vivo context including (2) extramuscularly connected muscle and (3) epimuscularly connected muscle) studied with 3 cases (passive isometric muscle with imposed relative position change (Case I),

passive lengthened muscle (Case II), and active isometric muscle with imposed relative position change (Case III): The findings indicated non-uniform strains for all models except for zero strain in model (1) in Case I, but models (2) and (3) also showed strains opposing the imposed effect, and effects get more pronounced with stiffer epimuscular connections. Assessments of forces exerted on the muscle by the epimuscular connections showed that such strain heterogeneities are ascribed to epimuscular myofascial loads determined by muscle relative position changes.

Chapter 4 Cankaya A.O., Yucesoy C.A., 2022. "Finite element modeling shows that epimuscular myofascial loads manipulate the effects of active state titin on mechanics of muscle integrated with its surroundings" submitted to Biomechanics and Modeling in Mechanobiology. Hypothesis was that compared to truly isolated muscle, for integrated muscle active state titin's effects on muscular mechanics are manipulated by EMFT. Isolated vs. integrated rat extensor digitorum longus muscles were modeled at long muscle lengths ( $l_m = 28.7\text{mm} - 32.7\text{mm}$ ) and three cases were studied: passive state titin (no change in titin constitutive equation in the active state), active state titin-I (constitutive equation involves a higher stiffness in the active state) and active state titin-II (constitutive equation also involves a strain shift coefficient accounting for titin's reduced free spring length). For isolated muscle, shorter sarcomere effect and force enhancement (maximally 77.4%) was consistent. However, for integrated muscles, variable fiber direction strains showed even longer or shortened sarcomeres locally and consequently, force enhancement was inconsistent being even diminished (7.8%) or elevated (96.8%) at different lengths. Shift of muscle's optimum length to a longer length in isolated muscle ( $l_m = 29.6\text{mm}$ ) increased ( $l_m = 29.9\text{mm}$ ) or vanished ( $l_m = 28.7\text{mm}$ ) for extra- or epimuscularly connected muscles, respectively. In conclusion, in the integrated muscle context, effects of active state titin on muscular mechanics are manipulated by EMFT.

## 2. The effects of an activation-dependent increase in titin stiffness on whole muscle properties using finite element modeling

### 2.1 Introduction

The two-myofilament model of the sarcomere characterizing its active force production based on the degree of overlap between actin and myosin[4],[3] has long been used to explain various muscle physiology phenomena[1][2]. Titin is a large protein[12], which from its N terminus at the Z-line to its C terminus at the M-line[14] spans the half-sarcomere, and is associated with sarcomere integrity[24] and has been considered as the source for intracellular passive tension[20][19]. In skeletal muscle, titin's elasticity stems from its elastic I band, which is comprised of Ig tandems, N2A, and proline glutamate valine lysine (PEVK) segment (see Nishikawa (2016) for illustrations of titin structure). Yet, the two-myofilament model plus passive elastic properties of titin could not explain certain muscle contraction phenomena involving excessive muscle forces, encountered in static stiffness[7] and residual force enhancement[8],[9]. That has led to the consideration of a different role for titin, as a part of the contractile machinery. Several studies investigated titin's structural changes upon muscle activation[39],[38],[40] and characterized its interactive role in muscle contraction[29],[6]. Primarily, titin was shown to have calcium affinity[34], which in the active state alters its configuration and properties imposing changes to its mechanical behavior[35],[18],[29].

Molecule-based studies identified sensitivity characteristics of the proline-glutamate-valine-lysine (PEVK) region of titin to calcium transients indicating titin changes structure as it interacts with calcium[35]. This region is a substantial contributor of titin's elasticity[55], especially in longer lengths, and its calcium affinity leads to an observed stiffness increase. Tests involving isolation of muscle fibers from actin-myosin interaction through chemical treatment allowed association of an excess force observed to titin's stiffness increase due to this calcium sensitivity[35].

Studies revealed that titin also has an interactive role in the contraction[56],[29],[6]. Skeletal muscles express N2A isoform, which is known to be another calcium sensitive region of titin[57]. Muscular dystrophy with myositis (mdm) mutation is known to be disrupting the N2A region of titin[58]. Studies on mice with mdm mutation enabled characterization of the N2A region[37]. It was shown for the mechanical behavior of active state titin that the mechanism, which includes the N2A region is more complex than only calcium induced stiffening[43]. As this involves titin-actin binding as well, a reduced free spring length of titin, hence a more complex mechanical behavior characterized by a shift of titin’s stress-strain characteristics was indicated[37],[43].

Despite those impressive advancements, active state titin’s effects have been studied predominantly in sarcomere, myofibril or muscle fiber segment level by measuring the force exerted[35],[37]. Therefore, assessment of functional effects in the muscle level are rare and recent[39],[40], moreover, an understanding of the mechanism of those in the context of a whole muscle is lacking. The linked fiber-matrix mesh model (LFMM)[59],[60] on the other hand is suitable for studying principles of those as it allows computationally establishing the mechanical equilibrium locally within the muscle as an interplay of constitutive behaviors of various muscle components, and provides metrics that characterize mechanisms of muscular force and movement production. Therefore, although single molecule or myofibril experiments do reveal the characteristic behaviors of active state titin, the LFMM can facilitate studying how those may alter within the whole muscle level and reflect onto muscular function. By representing active state titin’s elevated stiffness and shift of its stress-strain characteristics in the LFMM, our aim was to study the mechanism of effects and particularly to determine the functionally more effective active state titin model.

## 2.2 Methods

In the linked fiber-matrix mesh model (LFMM model), skeletal muscle is considered to consist of intracellular and extracellular matrix (ECM) domains. The trans-sarcolemmal attachments (multimolecular structures including dystrophin, dystrogly-

can complex and laminin) are considered as elastic links between the two domains[59][60]. Details about the model can be found in appendix A and in the corresponding article.

### 2.2.1 Isolated EDL Model

EDL muscle of the rat is a unipennate muscle with rather small pennation angles and minimal variation of the fiber direction within the muscle belly. The model geometry (Figure 2.1) is defined as the contour of a longitudinal slice at mid-muscle belly filled by three muscle elements in series and sixteen in parallel. Any collection of three muscle elements in series represents a muscle fascicle. Aponeurosis elements have identical mechanical properties, but increasing cross sectional area toward the tendon[61] is accounted for.

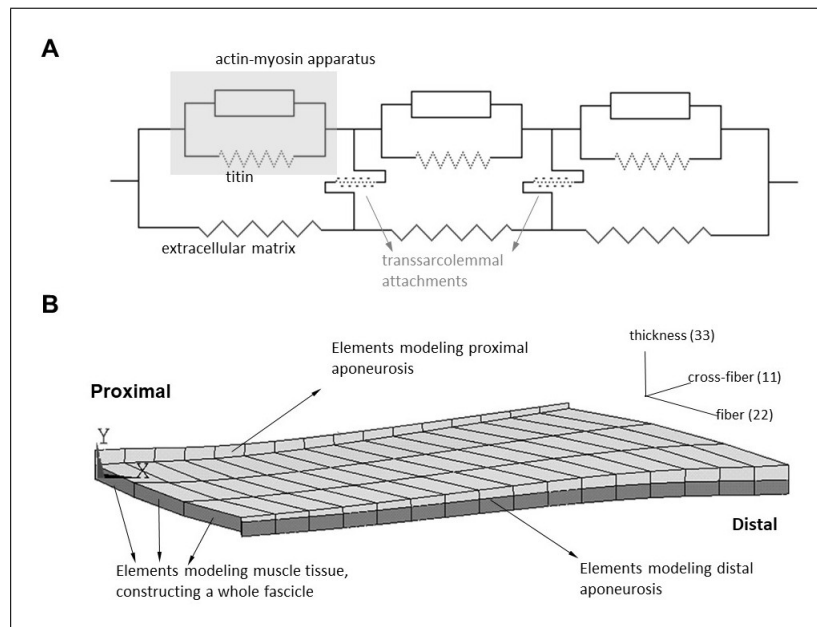


**Figure 2.1** Finite element model of EDL muscle of the rat. (a) Two dimensional schematic representation of an arrangement of muscle elements. The intracellular domain, which is comprised of the contractile apparatus and titin is linked to the extracellular matrix domain elastically through trans sarcolemmal attachments. (b) The model consists of three muscle elements in series and sixteen in parallel. Three muscle elements arranged in series construct a fascicle. A combination of nodes along one side of a fascicle is referred to as a fascicle interface. Each fascicle interface is indicated by a number from 1 to 17. The muscle elements located proximally and distally are connected to elements representing the muscles aponeuroses. A 3D local coordinate system representing the fiber, cross fiber (normal to the fiber direction), and thickness directions is used for the analysis and presentation of the model results[62]

### 2.2.2 Passive and active state titin cases

For  $\sigma_{22\text{titin}}$  in the passive state, experimental tension-sarcomere length data[20] for a single rabbit skeletal muscle fiber was fitted using a parabolic function and scaled to make it compatible to  $\sigma_{22\text{contr}}$ .

$$\sigma_{22\text{titin}}(\varepsilon_{22}) = t_1\varepsilon_{22}^2 + t_2\varepsilon_{22} + t_3 \quad (2.1)$$

and

$$\sigma_{22\text{titin}}(\varepsilon_{22}) = 0 \quad \text{for } \varepsilon_{22} = 0$$

where  $t_1$ ,  $t_2$  and  $t_3$  are constants (Table A.1). The reference model accounts for the passive state titin properties for also the active state, whereas the extended models distinguish and represent the principles of two possible components to titin's stiffness increase upon activation: a direct calcium-titin interaction[35] (active state titin-I), and a titin-actin interaction that reduces the free spring length[37] (active state titin-II). To incorporate the former, titin's stress-strain characteristics extracted from Labeit et al. (2003) were fit with a cubic polynomial.

$$\sigma_{22 \text{ titin}}(\varepsilon_{22}) = h_1\varepsilon_{22}^3 + h_2\varepsilon_{22}^2 + h_3\varepsilon_{22} \quad (2.2)$$

where  $h_1$ ,  $h_2$  and  $h_3$  are constants (Table A.1). To account for the latter, titin's stress-strain characteristics were manipulated by adding a shift coefficient  $\varepsilon_{\text{shift}}$ .

$$\sigma_{22 \text{ titin}}(\varepsilon_{22}) = h_1(\varepsilon_{22} - \varepsilon_{\text{shift}})^3 + h_2(\varepsilon_{22} - \varepsilon_{\text{shift}})^2 + h_3(\varepsilon_{22} - \varepsilon_{\text{shift}}) \quad (2.3)$$

Therefore, three cases utilizing Eqs. 2.1, 2.2, and 2.3, respectively were studied: (i) passive state titin, (ii) active state titin-I and (iii) active state titin-II. Corresponding stress-strain curves for these cases are shown in Figure2.2.

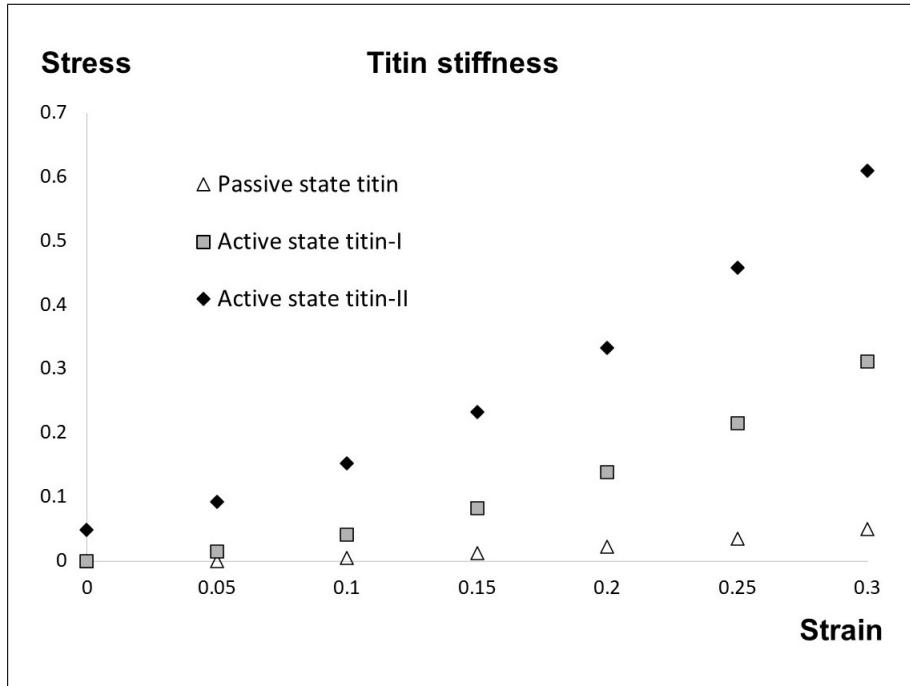


**Figure 2.2** The stress-strain characteristics of titin in the reference model (passive state titin) and extended models (active state titin-I and active state titin-II). Passive and active state resistance due to titin in the myofiber element is valid only in the local fiber direction

### 2.2.3 Solution procedure

For all models, initially, in passive state, the activation coefficient  $b_3 = 0$ . Maximal activation was achieved by increasing  $b_3$  incrementally up to 1, using fixed increments, while the muscle was kept at initial length ( $l_m = 28.7\text{mm}$ ). Muscle length was increased by changing the position of muscle distal end distally with 0.1 mm increments up to  $l_m = 32.7\text{mm}$ , while keeping the proximal end fixed (i.e., a muscle stretch approximating 14% was imposed). During the entire solution procedure, the models studied were stable and no mesh refinement was performed. A force-based convergence criterion was used with a tolerance of 0.5%.

### 2.2.4 Processing of data

Muscle length-total and active force (difference of passive and total muscle force) data were studied to quantify force enhancement.  $l_{mo}$  was determined as the length

at which muscle active force reaches its maximal value. All forces were normalized to the corresponding optimum force of the reference model.  $l_{mo}$  of active state titin cases were compared to that of the reference muscle.

Per muscle length: the mean nodal fiber direction strain per fascicle interface is considered to represent sarcomere length changes in active state titin cases vs. passive state titin case. Across muscle lengths: noting that  $\varepsilon_{22} = 0$  represents full myofilament overlap in sarcomeres, mean of absolute summed nodal strain value per muscle length over a range of muscle lengths represents an index for deviation from full myofilament overlap.

The mean nodal fiber direction stress per fascicle interface is considered to represent muscle force production changes in *active state titin* vs. *passive state titin* cases. Total stress,  $\varepsilon_{22\text{contr}}$  and  $\varepsilon_{22\text{titin}}$  were assessed separately. The area under mean nodal fiber direction stress-fascicle interface curves represents an index for force production.

## 2.3 Results

Fig. 3 shows muscle length-force characteristics for the three cases studied. Compared to passive state titin, active state titin-I elevates both muscle total and active forces (e.g., at 32.7 mm, by 14% and 38%, respectively). Active state titin-II causes an even more pronounced force enhancement both for total and active forces (e.g., at 32.7 mm, by 29% and 77%, respectively). However, remarkably, this is not the sole effect. Unlike the passive state titin case, which by definition, attains its maximum active force at  $l_m = 28.7\text{mm}$  and shows a force decrease with added muscle lengthening, active state titin-II shows that muscle active force keeps increasing for a certain muscle length range, causing the muscle's optimum length to shift to a longer length ( $l_m = 29.6\text{mm}$ ). Moreover, the plateau region of the curve is expanded (e.g., the force remains within 2% of the optimal force until  $l_m = 32.7\text{mm}$ ).

Figs. 4 and 5 show muscle fiber direction strains and stresses at  $l_m = 28.7\text{mm}$

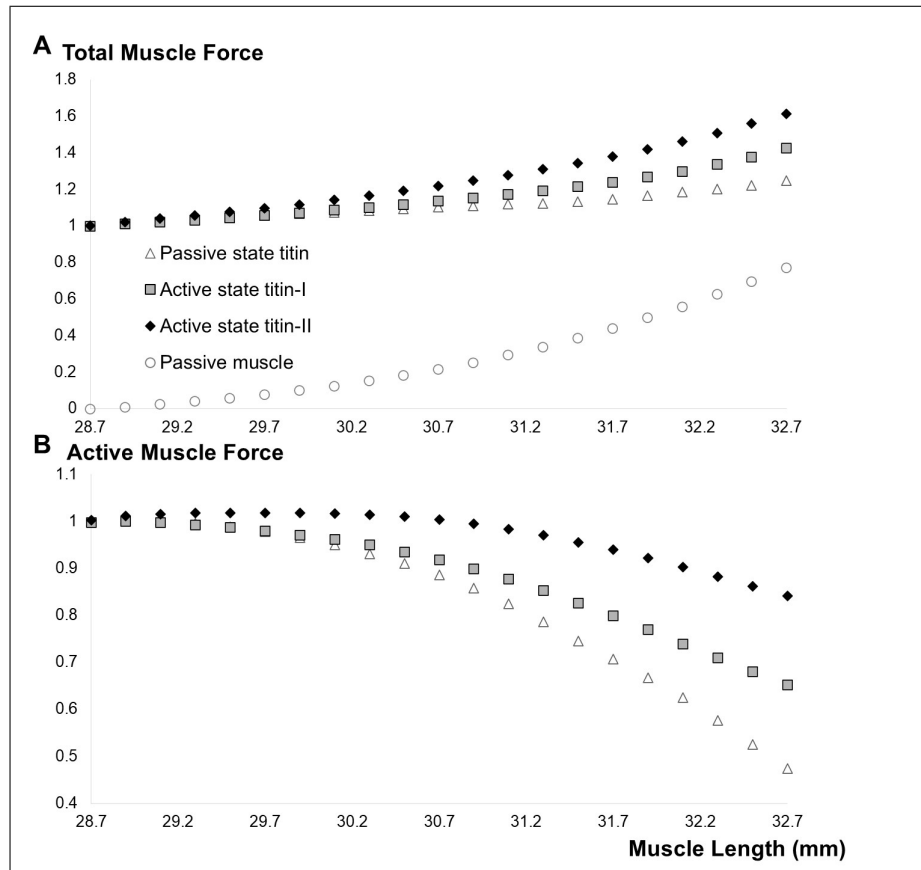


**Figure 2.3** The force-length characteristics of the modeled EDL muscles in the range of muscle lengths studied from initial length i.e.,  $l_m = 28.7\text{mm}$  to  $l_m = 32.7\text{mm}$ . (a) Total isometric muscle forces of different model cases are normalized to the optimum active force of the reference model. Passive muscle force-length characteristics of the modeled EDL muscles is shown. (b) Active isometric muscle forces of different model cases are calculated as the difference between total and passive muscle forces. Forces of the reference model (passive state titin) and extended models (active state titin-I and active state titin-II) are shown.

(the longest muscle length studied) and  $l_m = 28.7\text{mm}$  (the optimum muscle length for active state titin-II).

$l_m = 32.7\text{mm}$ : For all fascicle interfaces, mean fiber direction strain curve of active state titin-I (Figure 2.4a) is clearly localized below that of the passive state titin. Therefore, active state titin limits sarcomere lengthening (maximally by 10%, for fascicle interface 5). We will refer to this characteristic effect as shorter sarcomere effect (SSE). Compared to passive state titin, mean fiber direction total stress curve of active state titin-I is above that of the passive state titin (Figure 2.4b). Index for muscle fiber force production is higher by 31%, which is in concert with the force enhancement shown. This is ascribed to titin predominantly, but contractile index for force

production is also higher by 7% (Figure2.4c and Figure2.4d). The former is due to elevated titin stiffness, which despite limited lengthening yields greater stresses. The latter implies sarcomeres at the descending limb of their length-force curve exert more force compared to their counterparts in passive state titin case. Note that, SSE and its reflection to force production are even more pronounced for active state titin-II. Compared to passive state titin, sarcomere lengthening is limited further (maximally by 20%, for fascicle interface 5), index for muscle fiber force production is higher by 57% due predominantly to titin, but contractile index for force production is also higher by 15%.

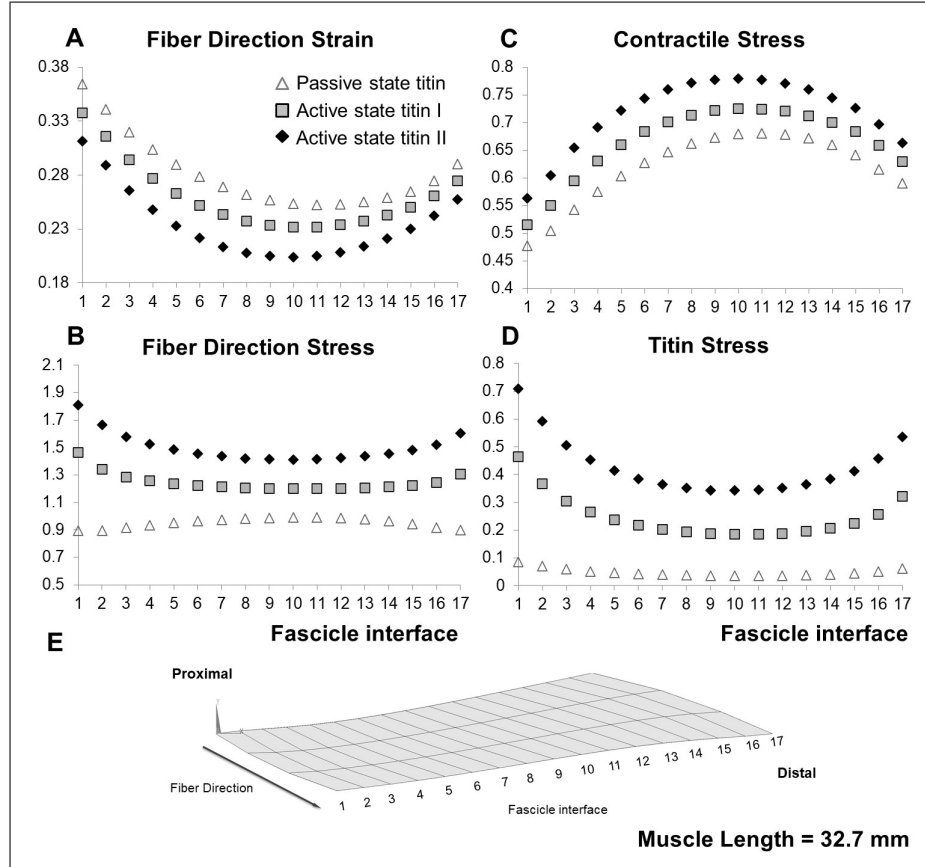


**Figure 2.4** Mean nodal fiber direction strain and stresses at  $l_m = 32.7\text{mm}$  per fascicle interface. Active state titin-I and II cases are compared to passive state titin case. (a) Mean fiber direction strain ( $\varepsilon_{22}$ ) across fascicle interfaces. (b) Mean nodal fiber direction contractile stress ( $\sigma_{22\text{CONTR}}$ ) across fascicle interfaces. (c) Mean nodal fiber direction titin stress ( $\sigma_{22\text{TITIN}}$ ) across fascicle interfaces. (d) Mean fiber direction total stress ( $\sigma_{22}$ ) across fascicle interfaces.

$l_m = 29.6\text{mm}$ : At the optimum muscle length for active state titin-II, SSE (Figure2.5a), and its reflection to force production (Figure2.5b - Figure2.5d) are lim-

ited to this case almost exclusively. Compared to passive state titin, sarcomere shortening is more pronounced (e.g., by 6.9% for fascicle interface 8). Index for muscle fiber force production is higher by 3% with contractile apparatus being the substantial contributor.

A distinctive effect for muscle lengthening as studied presently is that active state titin induced SSE allows keeping the sarcomeres closer to their full myofilament overlap, which is effective also beyond the shifted muscle optimum length of active state titin-II. For muscle lengths between  $l_m = 29.6\text{mm}$  and  $l_m = 32.7\text{mm}$ , index for deviation from full myofilament overlap for active state titin-II is 10% smaller than that of active state titin-I, which is 9% smaller than that of passive state titin.

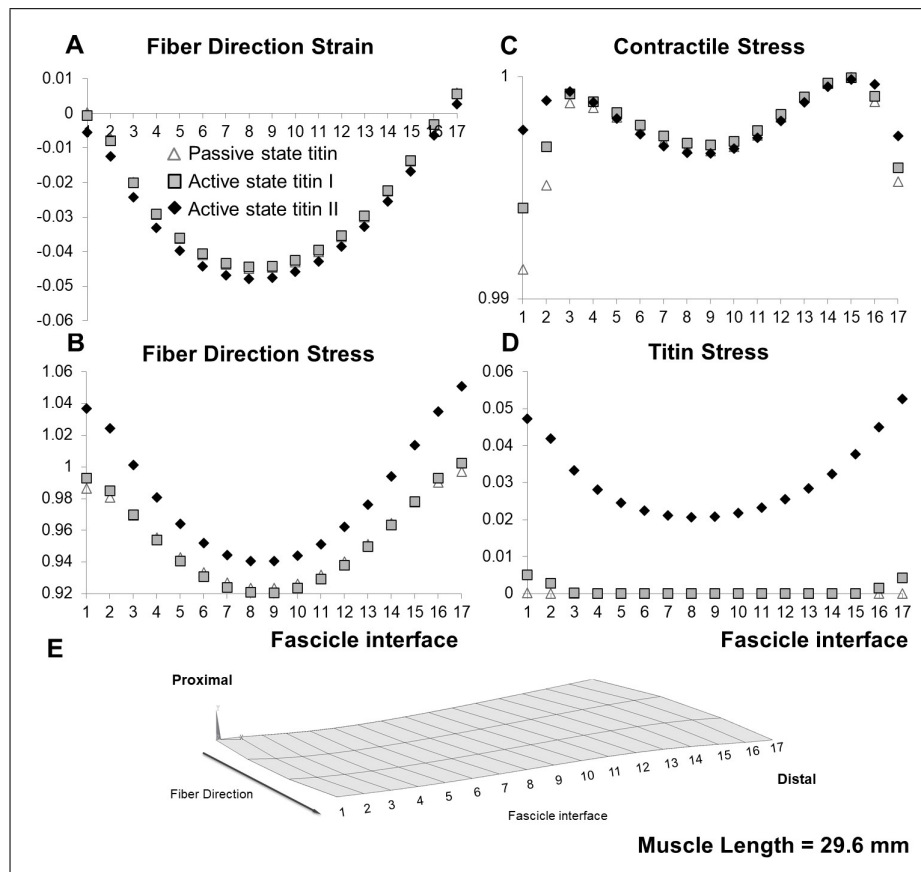


**Figure 2.5** Mean nodal fiber direction strain and stresses at  $l_m = 29.6\text{mm}$  per fascicle interface. Active state titin-I and II cases are compared to passive state titin case. (a) Mean fiber direction strain ( $\varepsilon_{22}$ ) across fascicle interfaces. (b) Mean nodal fiber direction contractile stress ( $\sigma_{22\text{CONTR}}$ ) across fascicle interfaces. (c) Mean nodal fiber direction titin stress ( $\sigma_{22\text{TITIN}}$ ) across fascicle interfaces. (d) Mean fiber direction total stress ( $\sigma_{22}$ ) across fascicle interfaces.

## 2.4 Discussion

Our aim was to determine the effect of activation-dependent titin stiffness on contracting skeletal muscle. The findings indicate the characteristic mechanism as the SSE. This mechanism underlies the well-known muscle force enhancement effect and not only because of the elevated contribution of the stiffer titin, but also because of the greater force development of the contractile element. However, a unique novel finding is that SSE also affects the muscle's length range of force exertion, causing a shift in optimum muscle length to a longer length. Notably, with more pronounced force enhancement and unique shift of optimum length effects, active state titin-II (reduced titin free spring length) is functionally more effective than active state titin-I (direct calcium stiffening of titin).

Previous studies assessing titin's role in the active state have been focused on two calcium-sensitive mechanisms. First is the stiffening of the PEVK region, which has a complex nature. PEVK region was shown to have a variable extensibility, with its N-terminal portion being most rigid and C-terminal being most flexible[63]. Moreover, presence of different conformational states were shown that enables fine tuning of protein interactions and elasticity, depending on conditions such as: temperature, polarity[64],[65], ionic strength[65], and calcium[35]. Obviously, calcium sensitivity of PEVK region is particularly interesting due to an association with the active state. Recombinant PEVK segments studied indicates that calcium binds to E-rich motifs with high affinity, yielding a stiffness increase in titin[35]. However, other studies have argued that the increase in PEVK stiffness cannot fully account for the increase in active muscle force with stretch[28],[43]. Second, is the titin-actin interaction: this is known to occur in cardiac myofibrils[66], described as a calcium-dependent interaction between PEVK-actin and is regulated by calcium-binding protein, S100A1[67]. This has been proposed as a mechanism for stress relaxation[68],[69] based on affected myofilament sliding via a viscous effect that can account for the transient decay of myofibril force in diastole. Titin-actin interaction was proposed to occur via the myosin-binding sites of actin[70],[71] and in the PEVK region of titin[72]. However, Dutta et al.[38] revealed that Ig domains within the N2A region are possible titin-actin binding sites. Mdm

mouse mutation tests characterized by 779-bp genomic deletion in the N2A region of titin, were utilized to investigate the role of that region in the active state[37]. This allowed prevention of extension of proximal Ig domain. Therefore, the PEVK region was left as the free-to-move portion of titin, yielding an increased stiffness response to stretching. N2A region was found to be the actin binding site of titin, and a reduction of titin's free-spring length was proposed as a consequence of such interaction with actin[37].

Remarkably, this effect was proposed to get further pronounced by actin's rotational movement upon myofilament contraction and a consequent winding of titin on actin. Therefore, in the sarcomere and myofilament level, the mechanical behavior of active state titin has been considered to involve several details. Moreover, there is considerable debate regarding those mechanisms. Ig-PEVK region's contribution to force in the physiologically relevant muscle length range in the passive state[29],[55] and its stiffness increase also in the active state is argued to be limited[35]. In contrast, the influence of actin-titin interaction on titin's stiffness increase was considered to substantiate in a way that allows titin to play a meaningful role in muscle force production and regulation[73],[6],[18]. Specific work is needed to better identify elements of those titin models[29]. However, the LFMM model is based on a continuum mechanics approach, which instead of accounting for the properties of individual components in such detail, takes into account generalized properties of lumped tissue components organized into finite elements and accounts for the steady-state elastic response. Therefore, overall, the modeled representation of active state titin phenomena is a major simplification of the molecular events. Note that, differences in mechanical properties between titin isoforms and contractile properties across different muscle types as well as species are conceivable[74],[75]. The reader is directed to the supplementary document for an addressing of effects of such variations.

Regarding representation of altered titin mechanical behavior in the active state, the present active state titin models both involve a higher stiffness than the passive state titin, which characterizes the calcium sensitive elevated stiffness of the PEVK region described in studies in sarcomere and myofibril level[35]. However, active state

titin-II also characterizes a reduction of titin's free-spring length by modeling an added shift of the stress-strain curve to smaller muscle fiber direction strain amplitudes. Yet, it does not model actin-titin mechanical interaction as described by [37] in isolation: in the LFMM model, actin and titin are considered in a parallel arrangement, hence the resistance of the muscle fiber domain to stretch is determined by the summed forces of the contractile apparatus and the titin. The higher stiffness of active state titin-II elevates titin's contribution to that force and this affects the length contractile apparatus attains. Resulting SSE is a key novel finding of the present study functional effects of which are addressed below. However, it is plausible that titin's winding on actin may not only lead to a reduction of titin's free-spring length, but also can change actin-myosin interaction. The present modeling currently does not account for such possible altered contractile apparatus mechanics. We consider that this is conceivably a very important mechanism yet; there is no general understanding of that available. The LFFM model can however, be used to assess the functional effects of that mechanism once it can be translated into constitutive equations characterizing the contractile apparatus.

A major contribution of the present continuum mechanics approach is the assessment of active state titin effects in the whole muscle level. This allows differently than previous fundamental studies conducted predominantly in much smaller levels, studying the functional effects at the muscle tendon along with their mechanisms within the muscle domain. A previously unconsidered functional effect of active state titin is a shift in muscle optimum length to a longer length, with a recent exception [41]. Effects of increased heterogeneity of sarcomere length distribution on widening of muscle's length range of force exertion via such shift was studied experimentally [76] and computationally [53][77]. However, presently this effect is not ascribed to altered heterogeneity of sarcomere lengths, but is in concert with the SSE. In previous studies, altered heterogeneity of sarcomere length changes involved local strain amplitude and direction changes [78],[79] due to altered amplitude and direction of myofascial loads originating from the ECM and connective tissues linking the muscle's belly to other muscles and non-muscular structures [54]. Such along muscle fiber length change heterogeneities were also studied in human muscle in vivo using magnetic resonance and

diffusion tensor imaging analyses[80],[81]. Our present findings indicate that as the characteristic effect of active state titin, SSE is encountered throughout the muscle belly without necessarily affecting strain heterogeneity. Functionally, SSE allows keeping the sarcomeres closer to their full myofilament overlap and is more pronounced for active state titin-II. For this muscle SSE is effective beyond a shift in muscle optimum length. As Figure 2.3 and the index for deviation from full myofilament overlap indicates, about 90% of muscle's optimal force production is observed for further muscle length increase imposed. More importantly, also beyond that, muscle's active force production is retained. Therefore, the SSE eliminates sarcomere overstretch and keeps the lengthening muscle from exhausting contractile force production. Structural determinants including a decrease in lattice spacing or a change in myosin structure for increased contractile force at longer lengths was recently reviewed[29],[6]. SSE cannot represent an adaptation, but indicates that the mechanical equilibrium is reached at a shorter sarcomere length. Note that the presently shown SSE, shift in muscle optimum length and retained heterogeneity of sarcomere lengths have notable relationships with recent titin centered studies reporting reduced sarcomere length heterogeneity with active stretch[56] and shifted muscle optimum length in wild type mice, unlike in titin deleted mdm mice[41]. The former suggests that in isolated muscle, increasing titin-based stiffness could potentially account for more sarcomere stability, which is in concert with the present model findings. Stable contractions and nearly homogeneous half-sarcomere lengths were shown to occur on the descending limb of the static total force-length relation also with elegant multi-scale continuum-mechanical modeling[82]. In the latter, mdm mice should also involve a disrupted completeness of trans-sarcolemal attachments and hence a compromised muscle fiber-ECM mechanical interaction. Findings of Hessel et al.[41] indicating a shifted muscle optimum length of tetanized muscle therefore, is ascribable to active state titin. However, we consider that for muscle operating in an intact muscle compartment in vivo, both muscle fiber-ECM, and muscle-surrounding structures mechanical interactions can further manipulate sarcomere length changes and hence, the functional effect of active state titin in the whole muscle level. Present modeling involves only maximal activation. Yet, along muscle fascicle strain heterogeneities were reported also for submaximal activation in vivo[81]. Such heterogeneity is conceivable to lead to e.g. a differential force enhancement effect

for different sarcomeres at different parts of the muscle. Note that, also the ECM[44] and aponeurosis properties[83] are likely to affect titin's influence on muscular force and movement production. These issues need to be further studied.

Active state titin's role on muscle's length range of force exertion is important for physiological muscle function, but is also highly relevant for pathological conditions such as cerebral palsy. One characteristic aspect of spastic muscle is a shift of its optimum muscle length to shorter lengths and sarcomere overstretch at longer ones[84],[85]. Our findings pose an interesting question as to whether a lack of active state titin mechanical influence may be responsible for the pathological spastic muscle function. Conceivable mechanisms may involve disrupted calcium-sensitivity of titin due to e.g., inefficient muscle activation. Recent intraoperative studies show that maximally activated spastic gracilis[86], semitendinosus[87] and semimembranosus[77] don't show low forces in extended knee positions, where the muscles are lengthened. However, intermuscular interactions[54] can manipulate titin's mechanical influence. Myofascial loads arising from stretching of connective tissue structures such as neurovascular tracts interconnecting muscles may affect the mechanical equilibrium between the contractile elements, titin and the ECM in determining muscle fiber direction length changes. Co-activation intraoperatively of synergistic and antagonistic muscles did change spastic gracilis[88],[89] and semitendinosus[90] forces leading in some cases to decreased force at longer muscle lengths. New studies are indicated to study these issues in nonisolated muscle to further explore active state titin's functional effects in a larger scale.

In conclusion, the present modeling indicated that shorter sarcomere effect is central to the mechanism of effects of active state titin, which becomes more pronounced and functionally more effective if not only calcium induced stiffening but also a reduced free spring length of titin is accounted for.

### 3. Principles of the Mechanism for Epimuscular Myofascial Loads Leading to Non-uniform Strain Distributions Along Muscle Fiber Direction: Finite Element Modeling

#### 3.1 Introduction

Muscle has a multi-scale composite structure[91]: its fundamental force producing units, sarcomeres, are connected to each other serially at z-discs[92], making up myofibrils, while adjacent myofibrils are interconnected and are also connected sequentially to laminin, the basal lamina, and endomysium via multimolecular and costameric proteins[93],[94],[95], which forms a three-dimensional structure in which muscle fibers operate[96]. Therefore, it is representative to consider skeletal muscle in a mechanically linked bi-domain concept of activatable muscle fibers and the extracellular matrix (ECM)[59]. Intramuscularly, this concept allows mechanical interaction of these domains such that local length changes along the muscle fiber direction is determined by the mechanical equilibrium affected by forces (myofascial loads) exerted by the ECM and other muscle fibers. The role of the ECM in limiting shortening of sarcomeres in an activated muscle fiber[97] and in limiting elongation of sarcomeres in passively stretched muscle fibers[97] was shown.

Additionally, all along the muscle belly, the ECM is continuous with structures outside the muscle: collagen reinforced connective tissue structures supporting the neurovascular tracts (i.e., the tissues containing nerves and blood vessels), compartmental boundaries, intermuscular septa, interosseal membrane, and the bone are in continuity and there is connectivity between the epimysia of adjacent muscles. This connective tissue integrity (for pictures, see, e.g.,[98],[99],[79],[100],[101], [102]) allows for transmission of forces to and from the muscle through non-tendinous pathways. Extramuscular connections are defined to represent muscle's connections to non-muscular structures exclusively. Epimuscular connections are defined to represent muscle's connections to both surrounding non-muscular and muscular structures. Therefore, extramuscular

and epimuscular myofascial loads can also affect the mechanical equilibrium determining local length changes along the muscle fiber direction. The mechanical interactions of the muscle with its surrounding muscular and non-muscular structures together are referred to as epimuscular myofascial force transmission (EMFT)[103],[54].

Previously, effects of such myofascial loads have been shown to cause, e.g., proximo-distal muscle force differences and mechanical condition dependent muscle length-force characteristics in animal studies as well as length change inhomogeneities along muscle fascicles in accompanying finite element modeling studies[52],[53]. Moreover, in vivo human studies using elastography[104] and magnetic resonance imaging (MRI) analyses[105] have shown that knee joint angle change imposed at restrained ankle angle causes non-uniform changes in the local stiffness and local length distributions of soleus muscle, respectively. Further studies combining diffusion tensor imaging (DTI) tractography to determine directions of muscle fascicles combined with MRI deformation analyses underlined the possibility of non-uniform deformations along muscle fascicles occurring in vivo under both passive and active conditions[80],[81]. Yet, mechanical principles of the mechanism behind the findings reported require further elaboration. Specifically, two questions arise from those findings regarding the muscle's length change heterogeneities along the muscle fiber direction: (1) How can a passively lengthened muscle show shortened regions? (2) How can an isometrically contracting muscle show lengthened parts? By studying principles of the mechanism of strain heterogeneity along the muscle fiber direction, the aim was to test the following hypothesis: epimuscular myofascial loads can lead locally to strains opposing those elsewhere within the muscle that are determined by the globally imposed conditions. For this purpose, finite element modeling was used and muscle fiber direction strains within a truly isolated muscle vs. those of extra- and epimuscularly connected muscles were studied in passive and active conditions.

## 3.2 Materials and Methods

### 3.2.1 Description of the "Linked Fiber-Matrix Mesh Model"

In the linked fiber-matrix mesh (LFMM) model, skeletal muscle is considered explicitly as two separate domains: (1) the intracellular domain and (2) ECM domain. The trans-sarcolemmal attachments are considered as elastic links between the two domains[59],[60]. Details about the model can be found in appendix A and in the corresponding article. The model geometry is given in (Figure3.1).

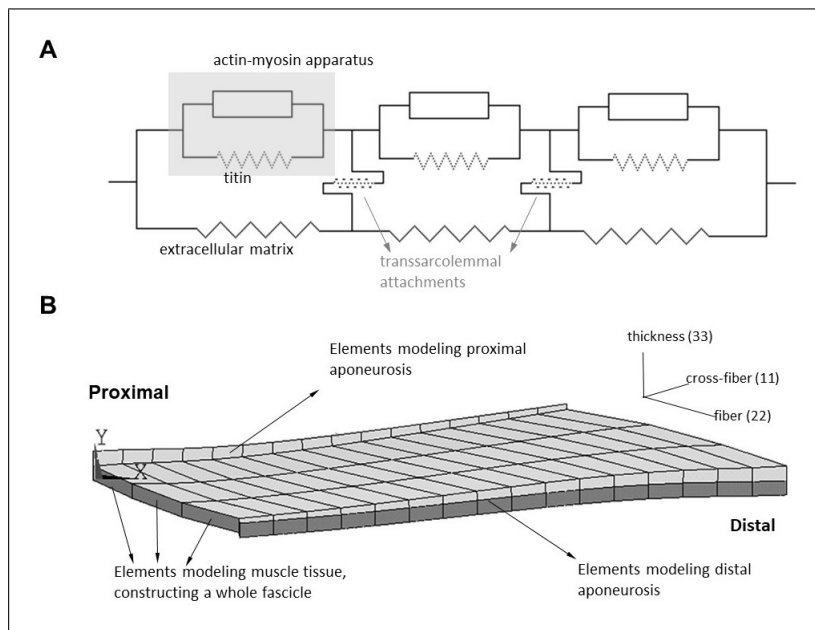


**Figure 3.1** Finite element model of EDL muscle of the rat. (a) Two dimensional schematic representation of an arrangement of muscle elements. The intracellular domain, which is comprised of the contractile apparatus and titin is linked to the extracellular matrix domain elastically through trans sarcolemmal attachments. (b) The model consists of three muscle elements in series and sixteen in parallel. Three muscle elements arranged in series construct a fascicle. A combination of nodes along one side of a fascicle is referred to as a fascicle interface. Each fascicle interface is indicated by a number from 1 to 17. The muscle elements located proximally and distally are connected to elements representing the muscles aponeuroses. A 3D local coordinate system representing the fiber, cross fiber (normal to the fiber direction), and thickness directions is used for the analysis and presentation of the model results[47]

### 3.2.2 LFMM Model Features and Definitions

Muscle length is defined as the distance between the proximal and distal muscle ends (Figure 3.2). Initial muscle length equals 28.7 mm. Three muscle elements in-series define a large fascicle (bundle of muscle fibers) and 16 fascicles in-parallel make up the muscle. An isometric condition describes an analysis in which the proximal and distal muscle ends are fixed; hence, the muscle length is globally kept constant. However, muscle fascicles run between the proximal and distal aponeuroses and can locally deform depending on the mechanical conditions imposed. It is assumed that, at the initial muscle length in the passive state, the sarcomeres arranged in series within muscle fibers have identical lengths. Local strain, as a measure of change of length, reflects the lengthening (positive strain) or shortening (negative strain) of sarcomeres. Note that zero strain in the model represents the undeformed state of sarcomeres (i.e., sarcomere length  $\approx 2.5\text{mm}$ ) in the passive condition at initial muscle length. Fiber direction strain within the fiber mesh of the LFMM model was used to assess the non-uniformity of lengths of sarcomeres arranged in-series within muscle fibers (referred to as serial distribution).

### 3.2.3 Muscle Models Studied

Extensor digitorum longus (EDL) muscle of the rat was modeled. This muscle is a unipennate muscle with a minimal variation of muscle fiber direction within the muscle belly. The muscle's relatively simple geometry is suitable for the present modeling focused on assessment of effects of epimuscular myofascial loads on local muscle strains. The geometry of the model was defined by the contour of a longitudinal slice at the mid-muscle belly. Three models were studied:

1. *Isolated muscle*: This muscle was kept fully isolated from its surroundings.
2. *Extramuscularly connected muscle*: In order to model the muscles' extramuscular connections (Figure 3.2A) and to account for their continuity with the muscu-

lar ECM, a set of nodes of the matrix mesh were linked using spring elements (COMBIN39, from the element library of ANSYS 12.0) to a set of fixed points (Figure 3.2B). In a previous experimental and anatomical study, the location of the extramuscular connections of the EDL muscle were determined to be at one-third of the fascicle length from the most proximal side of each muscle fascicle[52]. In the muscle mechanics part of that study, those connections were dissected to a maximum possible extent, without endangering circulation and innervation and the part supporting the neurovascular tract to the EDL were shown to be much stiffer than the rest of the connective tissues. Taking into account those previous findings, our modeling considerations were: (1) the set of fixed points comprising "mechanical ground" represent bone, which is assumed to be rigid. (2) The spring elements modeling the muscles' extramuscular connections were set to be uniaxial and have linear length-force characteristics. (3) Initially (i.e., muscle length = 28.7mm, and before changing any of the tendon positions), the fixed points and the corresponding nodes of the model were at identical locations (i.e., the spring elements modeling the muscles' extramuscular connections were at a length of zero). (4) The higher stiffness of the connective tissues constituting the neurovascular tract is taken into account by making the seven most proximal links to the muscle stiffer than the distal ones. Stiffness values determined previously[52] were used for the more compliant linkages, whereas a higher stiffness is preferred for the proximal ones (i.e.,  $k = 0.25$  unit force/mm for stiffer proximal part and,  $k = 0.033$  unit force/mm for the remaining links).

3. *Epimuscularly connected muscle*: This model aims at representing the principles of a muscle in its in vivo context. Hence, it includes the muscle's extramuscular connections together with intermuscular connections to neighboring muscle. In order to achieve that, two muscle models with geometries identical to that in (1) were intermuscularly connected: the corresponding nodes of the matrix meshes of the two models were linked elastically along their medial faces (Figure 3.2C). Extramuscular linkages remained in the lateral faces of each model. For both inter- and extramuscular links, the spring element COMBIN39 was used with linear stiffness characteristics. A suitable stiffness value ( $k = 0.2$  unit force/mm) was

used for the intermuscular elements to provide sufficient mechanical interaction between modeled muscles.

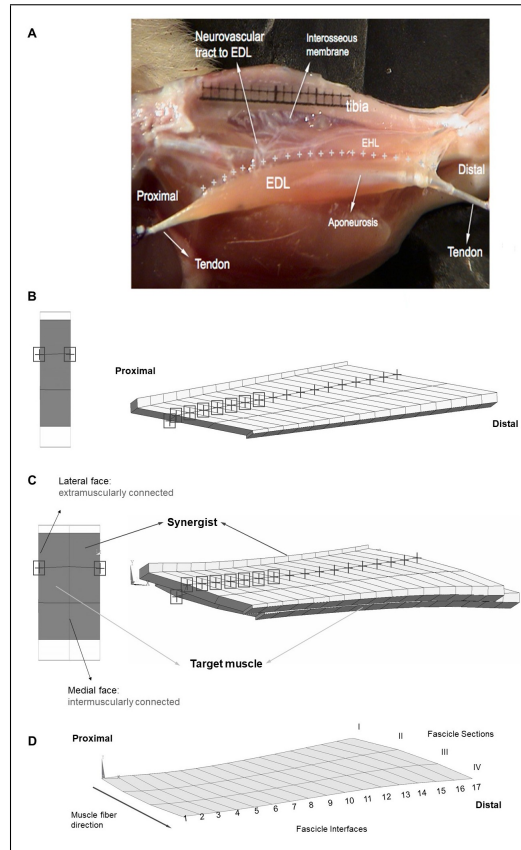


**Figure 3.2** Anatomy and geometry of the model cases studied. (A) An image adapted from a previous experimental and anatomical study[52]. The EDL is shown after removal of the tibialis anterior muscle of the anterior crural compartment, whereas the other muscle, EHL is not removed in this image. Extramuscular connections connect the EDL all along the muscle (marked by "+" signs) to the tibia, part of interosseal membrane and anterior intermuscular septum. This structure includes the neurovascular tract (i.e., the connective tissue structure containing nerves and blood vessels) and comprises a pathway of extramuscular myofascial force transmission. The geometry of modeled muscles is defined by the contour of a longitudinal slice of the rat EDL muscle belly (B,C). Three muscle elements in-series define a large fascicle and sixteen fascicles in-parallel make up the muscle. Fascicles terminate in rigidly linked aponeurosis elements, which increase in thickness toward tendon ends. (B) Extramuscularly connected muscle. The nodes of the matrix mesh marked by a black "+" sign have extramuscular connections to mechanical ground and the nodes marked also by a black square have stiffer connections. A proximal view in the undeformed state is shown on the left-hand side. Locations of the extramuscular connections are indicated using the same symbols as in the view of the longitudinal plane. (C) Epimuscularly connected muscle. The target muscle is intermuscularly connected to the synergist muscle: the corresponding nodes of the matrix meshes of the two models are linked elastically along their medial faces (shown by black circles on the left-hand side). The synergist is kept at a fixed length, whereas the target muscle is lengthened distally. Both of the models are also connected extramuscularly: the nodes of the matrix mesh marked by a black "+" sign have connections to mechanical ground. The nodes marked also by a black square have stiffer extramuscular connections. A proximal view of the models in the undeformed state is shown on the left-hand side. Also in this view, the location extramuscular connections of the model are marked. (D) Fascicle sections I-IV and fascicle interfaces 1-17 are associated with model geometry.

### 3.2.4 Cases Studied

In order to assess the effects of extra- and epimuscular myofascial loads on local length changes along the muscle fiber direction, three different cases were studied (Figure 3.3):

#### **Case I: Passive Isometric Muscle, With Imposed Relative Position Changes**

All three muscle models were studied in the passive state. The target muscles' length was kept constant at the initial muscle length. However, relative position changes were imposed for extra- and epimuscularly connected ones in order to assess the effects of myofascial loads developed on muscle fiber direction strains. Implementation: the proximal and distal ends of the target muscle were displaced distally by 2 mm.

#### **Case II: Passive Lengthened Muscle**

All three muscle models were studied in the passive state. The target muscles were further lengthened distally, which for the extra- and epimuscularly connected ones also elevates myofascial loads via more pronounced muscle relative position changes. Implementation: Subsequent to the relative position change imposed as described above, the target muscle's distal end was displaced distally by 2 mm.

#### **Case III: Active Isometric Muscle, With Imposed Relative Position Changes**

All three muscle models were fully activated, and their lengths were kept constant at the initial muscle length. However, relative position changes were imposed for the extramuscularly connected muscle and the epimuscularly connected target muscle, in order to assess the effects of myofascial loads developed on muscle fiber direction strains. Implementation: the proximal and distal ends of the target muscle were dis-

placed distally by 2 mm.

Note that Case I actually does not even involve any muscle lengthening, but aims at showing that solely relative position changes may lead to occurrence in different parts of passive muscle with shortening as well as lengthening in muscle fiber direction due to myofascial loads. However, Case II does involve also muscle lengthening, which case directly addresses plausibility of shortened parts occurring within a passively lengthened muscle due to myofascial loads. Finally, Case III aims at plausibility of lengthened parts occurring within an activated isometric muscle. Note that this case represents a strict scenario for the specific aim as activated isolated muscle at initial length should involve exclusively shortening.

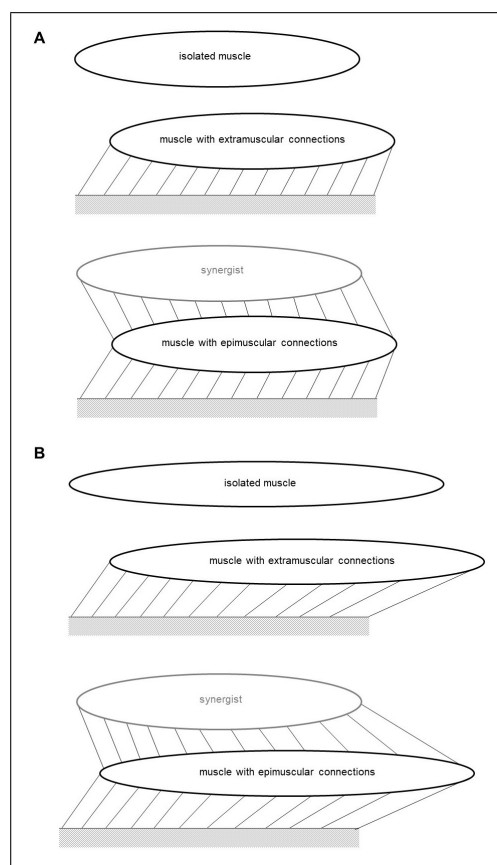


**Figure 3.3** Schematic representation of the protocols modeled. (A) Protocols for Case I and Case III. (B) Protocol for Case II. The links that connect the muscle to the mechanical ground represent the extramuscular connective tissue, and those that connect the muscle to the synergistic muscle represent the intermuscular connections. Extra- and epimuscularly connected muscles illustrate stretching of these links with imposed muscle relative position change (Cases I-III) and length imposed (Case II).

### 3.2.5 Solution Procedure

The analysis type used in ANSYS was static and large strain effects were included. During the entire solution procedure, the models studied were stable and no mesh refinement was performed. A force-based convergence criterion was used with a tolerance of 0.5%.

At the passive state, the activation coefficient  $b_3$  (EquationA.7) equaled 0 (for Cases I and II). For Case III, maximal activation of the muscles modeled was achieved by increasing  $b_3$  incrementally up to 1, using fixed increments.

### 3.2.6 Processing of Data

Local fiber direction strain indicated lengthening and shortening of sarcomeres, with zero strain representing the undeformed state of the sarcomeres.  $\varepsilon_{22}$  along nodes of serial fascicle interfaces (I-IV) were studied across fascicle interfaces 1-17 to quantify deformation patterns throughout muscle in isolated muscle, extramuscularly connected muscle, and epimuscularly connected muscle. For the epimuscularly connected muscle, the lateral, i.e., the extramuscularly connected face, and the medial, i.e., the intermuscularly connected face, were assessed separately.

Epimuscular myofascial loads were calculated as the fiber direction components of nodal reaction forces on the epimuscular linking elements, and assessed as normalized with respect to the largest epimuscular myofascial load value observed in the three cases studied. The epimuscular myofascial loads, which cause the most pronounced muscle fiber direction length changes, were presented.

### 3.3 Results

#### 3.3.1 Case I: Passive Isometric Muscle, With Imposed Relative Position Changes

Isolated isometric muscle shows the pre-defined zero strain condition as a reference for muscle with no myofascial loads acting on (Figure 3.4). In contrast, both extramuscularly and epimuscularly connected muscles show both shortening (Figure 3.4A,B -fascicle sections: I and II, maximally 35.3% in the lateral face of epimuscularly connected muscle), and lengthening (Figure 3.4C,D -fascicle sections: III and IV, maximally 23.6% in the medial face of epimuscularly connected muscle) in muscle fiber direction. For the lateral face of the epimuscularly connected muscle, which shows the most pronounced strain effects (Figure 3.4E), the myofascial loads (originating from extramuscular linking elements) are proximally directed owing to distally imposed muscle position changes. These loads, normalized with respect to the maximum epimuscular load calculated for Case II, range between 0.34 and 0.41 for the proximal nodes with stiffer extramuscular connections, and are below 0.09 for the remainder less stiff connections (Figure 3.4F). Despite the fact that no length changes were imposed globally on the muscle, these loads lead to shortening of the proximal part of the muscle (i.e., fascicle sections I and II). In return, the distal parts of the muscle (i.e., fascicle sections III and IV) show lengthening.

#### 3.3.2 Case II: Passive Lengthened Muscle

Isolated lengthened muscle shows lengthening in all fascicle interfaces, for all fascicle sections in muscle fiber direction (maximally by 28.7, 24.9, 19.6, and 23.0% in fascicle sections I-IV, respectively) (Figure 5). However, the extramuscularly connected muscle involves muscle fiber direction lengthening in most parts of the muscle but also shortening in some regions (fascicle section I in fascicle interfaces 1-7, up to 12.7%). This shortening effect is more pronounced in the epimuscularly connected muscle where shortening in the muscle fiber direction is shown in all fascicle interfaces of fascicle sec-

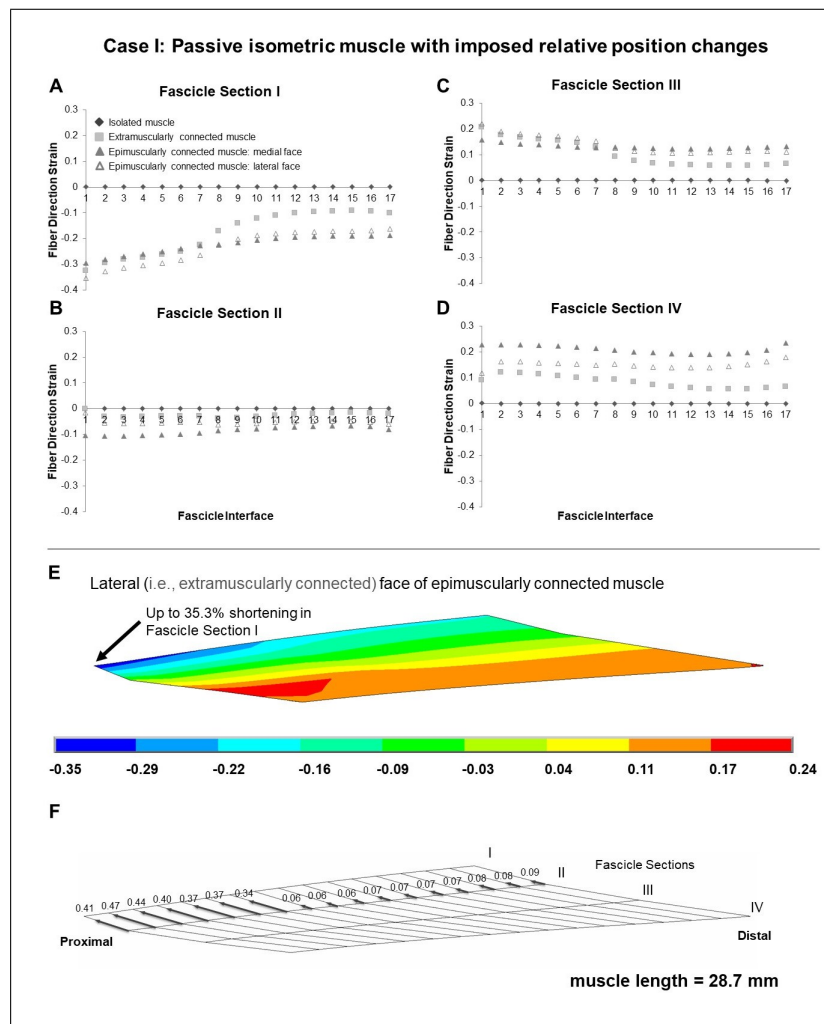


**Figure 3.4** Results presented for Case I: Passive isometric muscle, with imposed relative position changes. (A-D) Fiber direction strains after relative position change for passive target muscle at 28.7 mm length are plotted per fascicle sections I-IV for each fascicle interface 1-17 in isolated muscle, in extramuscularly connected muscle, in medial and lateral faces of epimuscularly connected muscle. (E) Color strain contour plots exemplified for epimuscularly connected muscle model's lateral face. The muscle parts that support the hypothesis are marked. (F) Myofascial loads due to extramuscular connections are calculated in local fiber direction, normalized with respect to the largest epimuscular myofascial load values observed in the three cases studied, and are depicted proportionately with glyphs on the lateral face of the target muscle.

tion I (maximally by 19.5% in the lateral face, Figure3.5E). Yet, presence of muscle fiber direction shortening is not the only difference. Compared to the isolated muscle, note also the different amplitudes of muscle fiber direction length changes shown in other parts: the extramuscularly connected muscle shows less pronounced muscle fiber direction lengthening in fascicle section I and II (maximally 19.2%, Figure3.5B) and more pronounced muscle fiber direction lengthening in fascicle section III and IV (maximally 38.0%, Figure3.5C). The epimuscularly connected muscle shows even lesser

pronounced muscle fiber direction lengthening in fascicle section II (maximally 16.1%, Figure3.5B) and even more pronounced muscle fiber direction lengthening in fascicle section III and IV (maximally 47.7%, Figure3.5D). These effects are ascribed to proximally directed epimuscular myofascial loads acting on these muscles (Figure3.5F shows those of the lateral face of the epimuscularly connected muscle). These loads range between 0.83 and 1 on the proximal nodes with stiffer extramuscular connections, and equal 0.13 for the majority of the remainder less stiff connections. As the muscles in this case are lengthened, the epimuscular myofascial loads manipulate the imposed muscle fiber stretch leading to elevation of lengthening in fascicle sections III and IV. However, they limit (fascicle section II) and even beat lengthening in the proximal parts of the muscle causing shortening fascicle section I.

### 3.3.3 Case III: Active Isometric Muscle, With Imposed Relative Position Changes

Isolated muscle shows only shortening regions upon isometric contraction, with an average strain of 10.0% (maximally by 12.2, 11.9, 12.2, and 13.0% in fascicle sections I-IV, respectively) (Figure3.6). In contrast, extra- and epimuscularly connected muscles show a more complex muscle fiber direction strain pattern including not only shortening, but also lengthening: (1) for fascicle sections I and II (Figures3.6A,B), both muscles show a more pronounced shortening compared to the isolated muscle (up to 33.3%). (2) On the other hand, for fascicle section III (Figure3.6C), both muscles show also certain lengthening in some fascicle interfaces (1-6 and 14-17, up to 5%). (3) Notably, for fascicle section IV (Figure3.6D), the epimuscularly connected muscle shows lengthening in both lateral (up to 16.8%) and medial (up to 23.4%, Figure3.6E) faces. These more complex muscle fiber direction strain patterns are ascribed to proximally directed epimuscular myofascial loads acting on these muscles. Figure3.6F shows those on the lateral face (ranging between 0.46 and 0.97 for the proximal nodes with stiffer extramuscular connections and below 0.15 elsewhere) and Figure3.6G shows those on the medial face (ranging between 0.33 and 0.12) of the epimuscularly connected muscle. As the muscles in this case are activated, the epimuscular myofascial loads manipulate

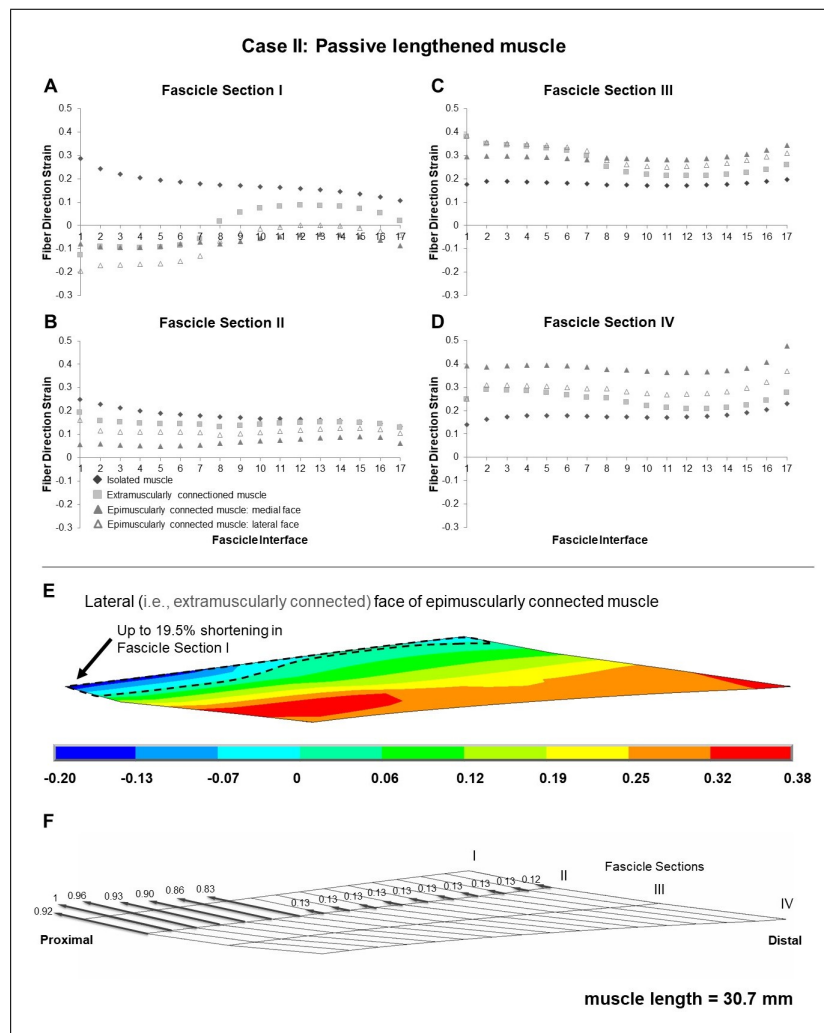


**Figure 3.5** (A-D) Fiber direction strains after relative position change for passive target muscle at 30.7 mm length are plotted per fascicle sections I-IV over fascicle interfaces 1-17 for isolated muscle, muscle with extramuscular connections alone, and for medial and lateral faces of muscle with inter- and extramuscular connections. (E) Color strain contour plots exemplified for epimuscularly connected muscle model's lateral face. The muscle parts that support the hypothesis are marked. (F) Myofascial loads due to extramuscular connections are calculated in local fiber direction, normalized with respect to the largest epimuscular myofascial load values observed in the three cases studied, and are depicted proportionately with glyphs on the lateral face of the target muscle.

the contraction-induced muscle fiber shortening. This leads to elevation of shortening in fascicle sections I and II as epimuscular myofascial loads shorten the proximal muscle elements. However, they limit and even overcome shortening as they stretch the distal muscle elements. This causes lengthening in fascicle sections III and IV.

Note that, further analyses (please see Supplementary Material) studying identical cases as above, but with higher stiffness inter- and extramuscular connections

yield more emphasized shortening in passively lengthened muscle and more emphasized lengthening in active isometric muscle, and the opposite for lower stiffness inter- and extramuscular connections. Those findings together with those of additional analyses studying effects of reduced imposed muscle length in Case II sustain the role of myofascial loads in manipulating local length changes along muscle fibers.

### 3.4 Discussion

The present modeling results indicate that muscle fiber direction strains in a truly isolated muscle and those in muscle in its in vivo context of connective tissue integrity would be very different. Note that, also for the truly isolated muscle, the findings show that muscle fibers operating within a whole muscle will not show a uniform muscle fiber direction strain distribution. This is because when the muscle's geometry and the boundary conditions are taken into account the mechanical equilibrium dictates length variations. For example, for an isometric muscle, muscle activation will not be able to cause shortening in the restrained muscle ends, hence the muscle fibers located proximally and distally shorten less than the ones located in the middle parts of the muscle belly. Moreover, if the muscle geometry is asymmetrical, the mechanical equilibrium dictates non-uniformity of the muscle fiber direction strains along the length of the muscle fibers. The presently modeled EDL muscle is asymmetrical and hence shows such length change variability. However, a truly isolated muscle fiber studied outside the muscle belly may show uniform strains along its length. This is bound to certain assumptions though. The muscle fiber's ends need to be fixed perfectly straight, so that no stress concentration occurs, which may, based on Saint Venant's principle in mechanics[106] alter the length changes at least within a part of the muscle fiber as long as its diameter. Also the mechanical properties of the muscle fiber need to be identical along its entire length. Nevertheless, the truly isolated muscle models studied presently did show one thing in common. That is, despite their non-uniformity, the muscle fiber direction strains were of the same direction, i.e., zero for Case I, all positive indicating lengthening for Case II, which involves a lengthened passive muscle and all negative indicating shortening for Case III, which involves an isometric activated muscle. In

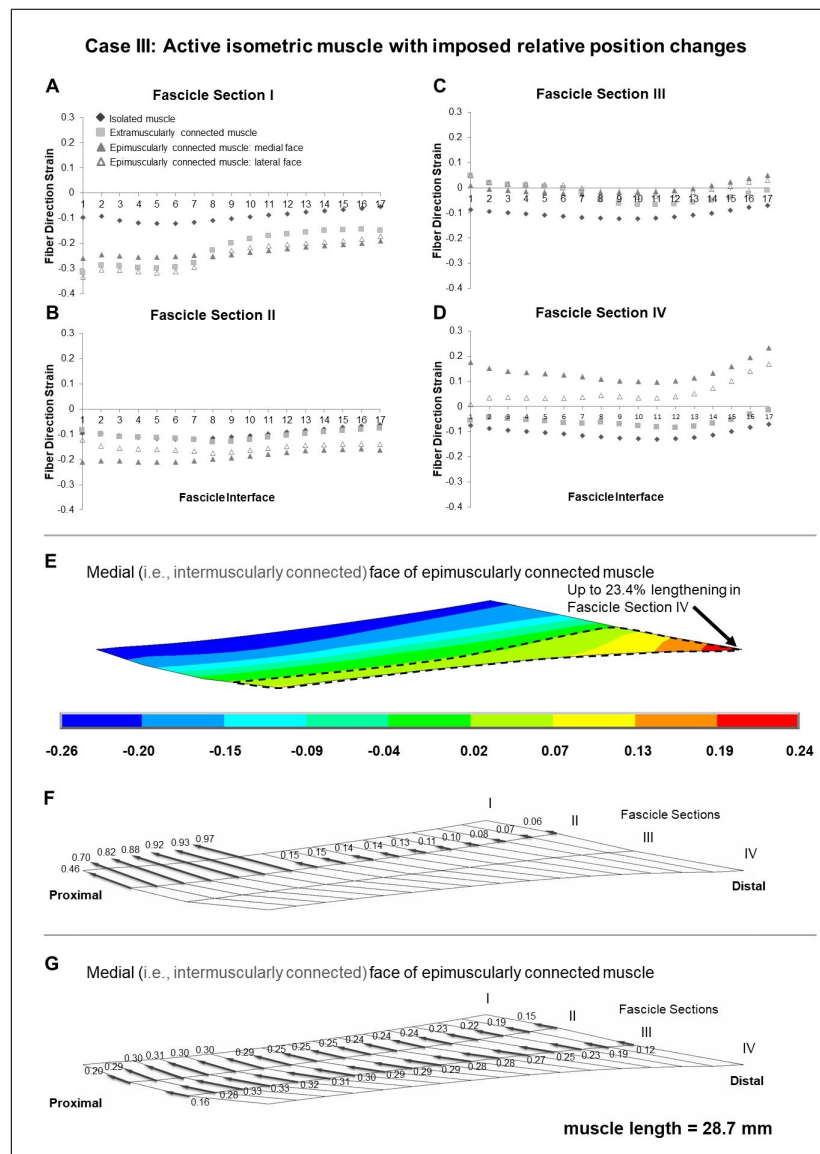


**Figure 3.6** Results presented for Case III: Active isometric muscle, with imposed relative position changes. (A-D) Fiber direction strains after relative position change for active target muscle at 28.7 mm length are plotted per fascicle sections I-IV for each fascicle interface 1-17 in isolated muscle, muscle with extra-muscular connections alone, and medial and lateral faces of muscle with inter- and extramuscular connections. (E) Color strain contour plots exemplified for epimuscularly connected muscle model's lateral face. The muscle parts that support the hypothesis are marked. (F) Myofascial loads due to extramuscular connections are calculated in local fiber direction, normalized with respect to the largest epimuscular myofascial load values observed in the three cases studied, and are depicted proportionately with glyphs on the lateral face of the target muscle. (G) Similarly, myofascial loads due to intermuscular connections are calculated and depicted proportionately with glyphs on the medial face of the target muscle.

contrast, the extra and epimuscularly connected muscles showed non-uniform muscle fiber direction strains, which typically involved also different strain directions as well. Findings, which may appear unexpected, are shown particularly in Case II featuring shortened parts in a lengthened muscle despite being passive and in Case III featuring

lengthened parts in a muscle, which is only activated without length changes imposed.

In addition to pioneering studies showing heterogeneous sarcomere lengths in human muscle *ex vivo*[107] and in animal muscle *in situ*[76], evidence on inhomogeneous length distribution of sarcomeres has accumulated for animal[108] and human[109] tibialis anterior muscle *in vivo* at multiple sites using second harmonic generation imaging. Therefore, sarcomere length measurements from a small region may not be representative of the entire muscle. A recent study in which tissue loading was imposed by joint angle changes has shown inhomogeneity of along muscle fiber strain distributions in human muscle upon passive extension of the knee[80]: MRI-based deformation analyses to determine local strains and DTI-based tractography to determine muscle fiber direction combined, the study showed that passively imposed proximal lengthening of human medial gastrocnemius (GM) yields both lengthened and shortened sections along the same fascicles. Using the same techniques, studying sustained submaximal isometric plantar flexion effort showed non-uniform strain distributions along muscle fascicles to include not only shortening but also lengthening[81]. Those effects were explained by EMFT in both studies: as locally epimuscular myofascial loads can affect the mechanical equilibrium, shortened muscle fascicle parts in a muscle stretch scenario and lengthened muscle fascicle parts in a muscle activation scenario was considered conceivable. This was supported by an assessment of local first principal strains within the segmented and visualized neurovascular tracts. Stretch on those collagen reinforced structures indicated exposure to epimuscular myofascial loads[81]. The locations within the GM where the neurovascular tracts were entering into the muscle were those that showed elevated muscle fiber direction length changes exemplifying the role of intermuscular mechanical interactions. Those strains were interpreted as sarcomere length changes along the GM fascicles *in vivo*. However, it must be noted that the resolution in these studies are in the order of millimeters, which is much coarser than the length of a sarcomere, and corresponds to sections of fascicle bundles. Also, the measurements involve strain, not length. Thus, strain non-uniformity found does not directly correspond to varying sarcomere lengths. Yet, these techniques are up-to-date assets: while DTI-based tractography alone is a powerful tool providing repeatable[110] anatomical information about human muscle fibers *in vivo* for both

upper[111] and lower extremity[112], coupling it with sequences providing tissue deformation or deformation rate such as cine phase contrast in order to achieve fiber direction information has been limited to few slices at a time (e.g., [113]). Time and subject's effort demands and more importantly dynamic nature of cine phase contrast-imaging experiments cause that. This technique yields tissue strains more directly[114] than MRI image registration techniques, but the resolution is low and an assumption is made that the static DTI acquisition represents the tissue properties at a selected joint angle during dynamic joint motion.

Techniques combining MRI and DTI analyses allow studying effects of intermuscular mechanical interactions in human muscles in vivo but as in other MRI modalities, provide kinematic information only. Although plantar-flexion force measured within the MRI scanner fed visually to the subject during acquisition[81] helped standardizing the subjects' sustained submaximal activation, the muscle force remains unknown. Therefore, in MRI analyses, an explanation of the findings based directly on force equilibrium of the muscle is not possible. However, finite element modeling allows addressing mechanical principles of that, and the present findings show the role of epimuscular myofascial loads on along muscle fiber strain distributions. It was pointed out recently[48] that such modeling may be used to elaborate on the findings of Pamuk et al.[80]. The present study accomplishes that by three model cases, which exemplify scenarios that yield uniform direction of strains if EMFT mechanism is ignored, and strains of opposite directions and heterogeneous amplitudes occurring along the same fascicles if it is not.

Note that human muscle studied in MRI analyses and the rat EDL model studied presently is not equivalent, but structural and muscle relative position differences exist. Regarding structure: the unipennate longitudinal EDL slice modeled bares important simplifications compared to complex geometries and properties of human muscles. The epimuscularly connected model involves two identical muscles with separate tendons, which is also a major structural simplification. Regarding muscle relative position changes: According to measurements in cadavers, 90° knee angle change results in 8% length change in GM[105], with 30° knee extension imposed in MRI analyses[80]

plausibly corresponding to 3-4% change in muscle length. Although presently modeled muscle lengthening approximates 7%, in the human study, the ankle kept at 90° also imposes a stretch on the GM suggesting that a comparable muscle lengthening is conceivable. However, intermuscular mechanical interactions must differ. Present epimuscularly connected model limits the mechanical interaction of the target muscle to that with an adjacent muscle only. Modeled muscles' interconnected faces provide direct, and neurovascular tracts connected at the mechanical ground provide indirect intermuscular interaction. In human, the target muscle is a part of the triceps surae with combined bipennate geometry and distally the muscles insert to the Achilles tendon, which also allows mechanical interaction[115]. Moreover, the intact limb provides mechanical interaction for the gastrocnemius muscles also with antagonistic muscles. Due to the preserved ankle position, proximally imposed lengthening changes of their position relative to the remainder lower leg muscles. Therefore, more pronounced intermuscular relative position changes and stretch on interconnecting connective tissue structures is plausible. Note that location and stiffness of such connections are conceivably different not only across muscles and species, but also among individuals. Therefore, the amplitudes and directions of myofascial loads differ in both studies. Please see Supplementary Material for model elaboration on extra- and epimuscular connection stiffness's and muscle relative position changes, which confirm the role of myofascial loads in the mechanism of along muscle fiber direction strain heterogeneity.

The rat EDL has been studied extensively experimentally[116],[117],[118],[119][120] and using matching finite element modeling[78],[53],[121],[52]. Therefore, a good understanding of its mechanics and anatomy forms sound basis for present modeling. Previous work on epimuscularly connected bi-articular rat EDL generated several new viewpoints suggesting implications of the present findings. Unequal proximal and distal forces is one characteristic finding[98] (Huijing and Baan, 2001). The force difference at each muscle length represents the net of epimuscular myofascial loads acting on the muscle belly. Modeling their effects inside the muscle led to an understanding that muscle length is not the sole determinant of isometric muscle force production. Instead, muscle relative position is a co-determinant because it manipulates epimuscular myofascial loads, which in return affect sarcomere lengths[78],[122],[52],[123]. Muscle fiber-ECM

mechanical interactions are the core of this mechanism, e.g., limiting sarcomere shortening in botulinum toxin type-A (BTX-A) treated muscle[124], which explains muscle length-dependent force reductions[125] and narrowing of muscle length range of force exertion[88]. Elevated ECM stiffness[126] yields more pronounced BTX-A effects in modeled due course of treatment[127]. Epimuscular myofascial loads studied presently are important because they interfere with muscle fiber-ECM mechanical interactions. This may make muscle's length-force characteristics vary in different conditions. It was shown intraoperatively in patients with cerebral palsy that spastic muscles' force amplitude can change significantly by co-activating other muscles[128],[89],[90].

### 3.5 CONCLUSION

In the present study, we developed finite element models and studied different cases to explore the principles of the mechanisms of non-uniform strain distributions along the muscle fiber direction with a particular emphasis on strains opposing the imposed effect as shown in previous human studies *in vivo*. Assessments of muscle fiber direction strains and forces exerted on the muscle by the epimuscular connections showed that such strain heterogeneities are ascribed to epimuscular myofascial loads determined by muscle relative position changes.

## 4. Titin EMFT Article

### 4.1 Introduction

Titin's role in the active force production has been widely studied in relation to its potential for explaining muscle mechanics phenomena where the two myofilament model fell short[129],[9]. A key finding was that titin has affinity to calcium[34], which further leads to mechanisms affecting titin's mechanical role: (I) a stiffness increase due to calcium binding to titin's PEVK region[35], and (II) titin-actin interaction via the N2A region[38], which also elevates titin stiffness by a reduction in its free spring length[37],[130]. Overall, a collection of findings in the literature support the idea that titin is an active component in force production[29],[6]. Subsequently, new and exciting contraction models taking titin into account such as the winding filament theory[37] and three-myofilament model[73],[56] were introduced. Recently, we have studied mechanical effects of those calcium dependent mechanisms with the aim to reveal mechanism of effects of active state titin and particularly to determine the functionally more effective one[131]. This showed that the characteristic mechanism comprises a limited lengthening locally along the muscle fiber direction, which was referred to as the shorter sarcomere effect. As a consequence, the effects of titin were shown to become more pronounced and functionally more effective if not only calcium induced stiffening, but also a reduced free spring length model is accounted for.

Note that, earlier experiments conducted were mainly in the myofibril/fiber level[28],[43] or on skeletal muscle[40] in-situ. It is important to also note that muscle in the in vivo context is not isolated from its surroundings. Instead, it has connections to the neighboring muscles and non-muscular connective tissues[49],[51], operating as an integral part of the fascial system[132],[133],[134]. It has been shown that muscle's extramuscular and epimuscular (i.e., collagen reinforced connective tissue structures including neurovascular tracts, general and compartmental fascia, intermuscular septa, interosseous membranes connecting muscle's epimysium to non-muscular structures

and also other muscles, respectively), connections affect not only the global mechanics of the muscle i.e., the muscle force[78],[79], but also locally the myofascial loads[47],[54] can alter the mechanical equilibrium determining length changes along the muscle fascicles[80],[81]. Principles of effects of such epimuscular myofascial force transmission (EMFT) leading to local muscle fiber direction length changes have been shown recently[135]. Consequently, compared to truly isolated muscle, we hypothesized for such integrated muscle that the role of active state titin as the third myofilament in muscular mechanics can be manipulated by EMFT. The present study aims to test this hypothesis by using the linked fiber-matrix mesh model (LFMM)[60],[124],[127].

## 4.2 Methods

In the LFMM model, skeletal muscle is considered to consist of intracellular and extracellular matrix (ECM) domains. The trans sarcolemmal attachments (multimolecular structures including dystrophin, dystroglycan complex and laminin) are considered as elastic links between the two domains[59],[60]. Details about the model can be found in appendix A and in the corresponding article.

Two user defined elements were developed in ANSYS 12.0: The ECM element represents the basal lamina, endomysium, perimysium and epimysium. The myofiber element models the muscle fibers. Both elements have eight nodes, linear interpolation functions and a large deformation analysis formulation. A 3D-local coordinate system representing the fiber, cross fiber and thickness directions is used. Separate meshes of ECM and myofiber elements occupying the same space are rigidly connected to single layers of aponeuroses and are linked elastically at intermediate nodes. In the LFMM model, one muscle element represents a segment of a bundle of muscle fibers, its connective tissues and the links between them (Fig.4.1A).

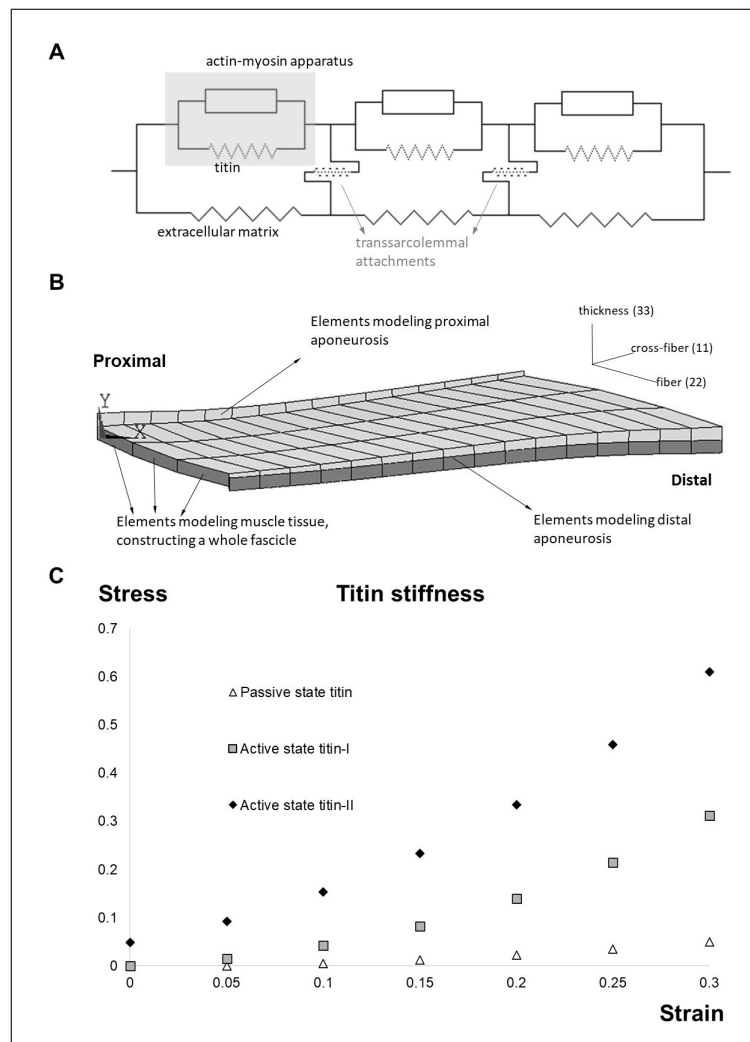


**Figure 4.1** (A) Two dimensional schematic representation of an arrangement of muscle elements. The intracellular domain, which is comprised of the contractile apparatus and titin is linked to the extracellular matrix domain elastically through trans sarcolemmal attachments. (B) The model consists of three muscle elements in series and sixteen in parallel. Three muscle elements arranged in series construct a fascicle. A combination of nodes along one side of a fascicle is referred to as a fascicle interface. Each fascicle interface is indicated by a number from 1 to 17. The muscle elements located proximally and distally are connected to elements representing the muscles aponeuroses. A 3D local coordinate system representing the fiber, cross fiber (normal to the fiber direction), and thickness directions is used for the analysis and presentation of the model results[62]. (C) The stress-strain characteristics of titin in the reference model (passive state titin) and extended models (active state titin-I and active state titin-II). Passive and active state resistance due to titin in the myofiber element is valid only in the local fiber direction

#### 4.2.1 Isolated EDL Model

EDL muscle of the rat is a unipennate muscle with rather small pennation angles and minimal variation of the fiber direction within the muscle belly. The model geometry (Fig.4.1B) is defined as the contour of a longitudinal slice at mid-muscle

belly filled by three muscle elements in series and sixteen in parallel. Any collection of three muscle elements in series represents a muscle fascicle. Aponeurosis elements have identical mechanical properties, but increasing cross sectional area toward the tendon[61] is accounted for.

#### 4.2.2 Extramuscularly Connected Model

In order to model the muscles' extramuscular connections (Fig.4.2A) and to account for their continuity with the muscular ECM, a set of nodes of the matrix mesh were linked using spring elements (COMBIN39, from the element library of ANSYS 12.0) to a set of fixed points (Fig.4.2B). In a previous experimental and anatomical study, the location of the extramuscular connections of the EDL muscle were determined to be at one-third of the fascicle length from the most proximal side of each muscle fascicle[52]. Accordingly, our model considerations were: (1) the set of fixed points comprising "mechanical ground" represent bone, which is assumed to be rigid. (2) The spring elements modeling the muscles' extramuscular connections were set to be uniaxial and have linear length-force characteristics. (3) Initially (i.e., muscle length = 28.7mm, and before changing any of the tendon positions), the fixed points and the corresponding nodes of the model were at identical locations (i.e., the spring elements modeling the muscles' extramuscular connections were at a length of zero). (4) The higher stiffness of the connective tissues constituting the neurovascular tract is taken into account by making the seven most proximal links to the muscle stiffer than the distal ones. Stiffness values determined previously[52] were used for the more compliant linkages, whereas a higher stiffness is preferred for the proximal ones (i.e.,  $k = 0.25$  unit force/mm for stiffer proximal part and,  $k = 0.033$  unit force/mm for the remaining links).

### 4.2.3 Epimuscularly connected muscle

This model aims at representing the principles of a muscle in its *in vivo* context. Hence, it includes the muscle's extramuscular connections together with intermuscular connections to neighboring muscle. In order to achieve that, two muscle models with geometries identical to that in (1) were intermuscularly connected: the corresponding nodes of the matrix meshes of the two models were linked elastically along their medial faces (Fig.4.2C). Extramuscular linkages remained in the lateral faces of each model. For both inter- and extramuscular links, the spring element COMBIN39 was used with linear stiffness characteristics. A suitable stiffness value ( $k = 0.2$  unit force/mm) was used for the intermuscular elements to provide sufficient mechanical interaction between modeled muscles.

### 4.2.4 Passive and active state titin cases

The *reference model* accounts for the passive state titin properties for also the active state, whereas the *extended models* distinguish and represent the principles of two possible components to titin's stiffness increase upon activation: a direct calcium-titin interaction[35] (active state titin-I), and a titin-actin interaction that reduces the free spring length[37] (active state titin-II).

To incorporate the former, titin's stress-strain characteristics extracted from Labeit et al. (2003) were fit with a cubic polynomial.

$$\sigma_{22} \text{ titin}(\varepsilon_{22}) = h_1 \varepsilon_{22}^3 + h_2 \varepsilon_{22}^2 + h_3 \varepsilon_{22} \quad (4.1)$$

where  $h_1$ ,  $h_2$  and  $h_3$  are constants (Table A.1).

To account for the latter, titin's stress-strain characteristics were manipulated by adding a shift coefficient  $\varepsilon_{\text{shift}}$ .

$$\sigma_{22} \text{ titin}(\varepsilon_{22}) = h_1 (\varepsilon_{22} - \varepsilon_{\text{shift}})^3 + h_2 (\varepsilon_{22} - \varepsilon_{\text{shift}})^2 + h_3 (\varepsilon_{22} - \varepsilon_{\text{shift}}) \quad (4.2)$$

Corresponding stress-strain curves for these cases are shown in Figure4.1C.

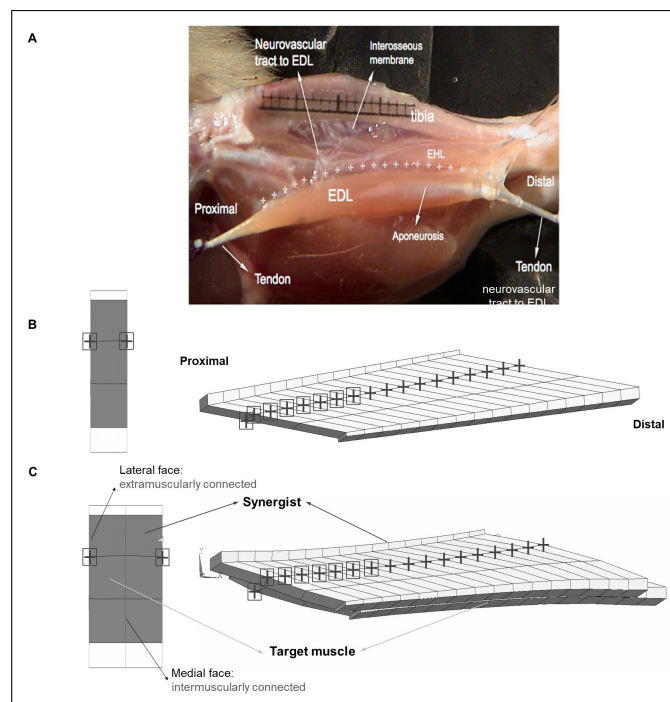


**Figure 4.2** Anatomy and geometry of the model cases studied. (A) An image adapted from a previous experimental and anatomical study[52]. The EDL is shown after removal of the tibialis anterior muscle of the anterior crural compartment, whereas the other muscle, EHL is not removed in this image. Extramuscular connections connect the EDL all along the muscle (marked by "+" signs) to the tibia, part of interosseal membrane and anterior intermuscular septum. This structure includes the neurovascular tract (i.e., the connective tissue structure containing nerves and blood vessels) and comprises a pathway of extramuscular myofascial force transmission. The geometry of modeled muscles is defined by the contour of a longitudinal slice of the rat EDL muscle belly (B,C). Three muscle elements in-series define a large fascicle and sixteen fascicles in-parallel make up the muscle. Fascicles terminate in rigidly linked aponeurosis elements, which increase in thickness toward tendon ends. (B) Extramuscularly connected muscle. The nodes of the matrix mesh marked by a black "+" sign have extramuscular connections to mechanical ground and the nodes marked also by a black square have stiffer connections. A proximal view in the undeformed state is shown on the left-hand side. Locations of the extramuscular connections are indicated using the same symbols as in the view of the longitudinal plane. (C) Epimuscularly connected muscle. The target muscle is intermuscularly connected to the synergist muscle: the corresponding nodes of the matrix meshes of the two models are linked elastically along their medial faces (shown by black circles on the left-hand side). The synergist is kept at a fixed length, whereas the target muscle is lengthened distally. Both of the models are also connected extramuscularly: the nodes of the matrix mesh marked by a black "+" sign have connections to mechanical ground. The nodes marked also by a black square have stiffer extramuscular connections. A proximal view of the models in the undeformed state is shown on the left-hand side. Also in this view, the location extramuscular connections of the model are marked.

#### 4.2.5 Solution procedure

For all models, initially, in passive state, the activation coefficient  $b_3 = 0$ . Maximal activation was achieved by increasing  $b_3$  incrementally up to 1, using fixed increments, while the muscle was kept at initial length ( $l_m = 28.7\text{mm}$ ). Muscle length was increased by changing the position of muscle distal end distally with 0.1 mm increments up to  $l_m = 32.7\text{mm}$ , while keeping the proximal end fixed (i.e., a muscle stretch approximating 14% was imposed). During the entire solution procedure, the models studied were stable and no mesh refinement was performed. A force-based convergence criterion was used with a tolerance of 0.5%.

#### 4.2.6 Processing of data

Muscle length-total and active force (difference of passive and total muscle force) data were studied to quantify force enhancement.  $l_{mo}$  was determined as the length at which muscle active force reaches its maximal value. All forces were normalized to the corresponding optimum force of the reference model.  $l_{mo}$  of active state titin cases were compared to that of the reference muscle.

Per muscle length: the mean nodal fiber direction strain per fascicle interface is considered to represent sarcomere length changes in active state titin cases vs. passive state titin case. Across muscle lengths: noting that  $\varepsilon_{22} = 0$  represents full myofilament overlap in sarcomeres, mean of absolute summed nodal strain value per muscle length over a range of muscle lengths represents an index for deviation from full myofilament overlap.

The mean nodal fiber direction stress per fascicle interface is considered to represent muscle force production changes in *active state titin* vs. *passive state titin* cases. Total stress,  $\varepsilon_{22\text{contr}}$  and  $\varepsilon_{22\text{titin}}$  were assessed separately. The area under mean nodal fiber direction stress-fascicle interface curves represents an index for force production.

## 4.3 Results

### 4.3.1 Local effects of EMFT, manipulating effects of active state titin

Figs. 4.3 and 4.4 show muscle fiber direction nodal strains in activated muscle in the distal (III and IV) and proximal (I and II) fascicle sections at  $l_m = 32.7\text{mm}$  for active state titin-I and active state titin-II (left and right panels, respectively).

#### Distal fascicle sections

*Active state titin effect:* typically, in isolated muscle, compared to passive state titin, active state titin leads to shorter sarcomeres (Fig. 4.3), which effect gets more pronounced for active state titin-II: e.g., maximally, 48.9% (passive state titin) vs. 41.4% (active state titin-I) and 38.3% (active state titin-II) for fascicle interface 17 (Fig. (Fig. 4.3)D). Exceptions exist limited to fascicle interfaces 1-3.

*EMFT manipulating effect:* in contrast, compared to isolated muscle, muscles with extra- and epimuscular connections show longer sarcomeres consistently: e.g., maximally, 20.4% vs. 37.4% for active state titin-I, fascicle interface 1 (Fig. (Fig. 4.3)B). For most fascicle interfaces, this vanishes the typical effect of active state titin.

#### Proximal fascicle sections

*Active state titin effect:* in isolated muscle, compared to passive state titin, active state titin leads to the typical effect of shorter sarcomeres (i) entirely in fascicle section II (Fig.4.4B) and (ii) for about half of fascicle section I (Fig.4.4A), which effect gets more pronounced for active state titin-II: for (i) maximally, 46.6% (passive state titin) vs. 40.6% (active state titin-I) and 37.0% (active state titin-II) for fascicle interface 1. For (ii) maximal shortening: 53.7% (passive state titin) vs. 46.9% (active state titin-I) and 43.3% (active state titin-II) for fascicle interface 1; maximal lengthening: 7.9% (passive state titin) vs. 14.0% (active state titin-I) and 14.3% (active state titin-II) for fascicle interface 17.

*EMFT manipulating effect:* Two main effects are shown, the latter being highly remarkable: (1) fascicle section II: compared to isolated muscle, muscles with extra- and epimuscular connections show shorter i.e., less lengthened sarcomeres consistently e.g., maximally, 46.6% vs. 17.7% for active state titin-II, fascicle interface 1 (Fig. 4.4D). For most fascicle interfaces, this makes the typical effect of active state titin more pronounced. (2) fascicle section I: again, compared to isolated muscle, muscles with extra- and epimuscular connections show shorter sarcomeres consistently, but instead of being less lengthened, this presents itself as even shortened sarcomeres. For fascicle interfaces 2-9 (Fig. 4.4A) and 2-8 (Fig. 4.4B), sarcomeres are shortened up to 9.8% in fascicle interface 6 (in contrast to 27.5% lengthening in isolated muscle).

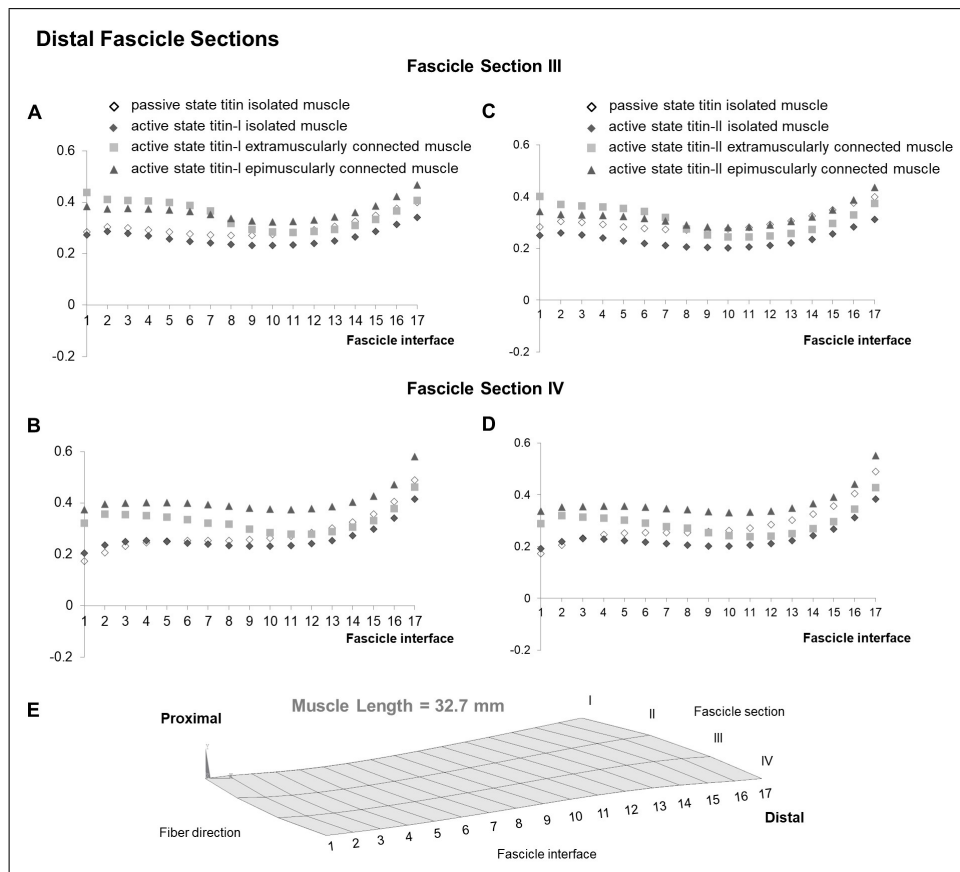


**Figure 4.3** Nodal fiber direction strains for distal fascicle sections (III-IV) at  $l_m = 32.7$  mm per fascicle interface. (A) (C) Active state titin-I and titin-II with isolated muscle, extramuscularly connected muscle, and epimuscularly connected muscle are compared to passive state titin with isolated muscle for fascicle section III. (B) (D) Active state titin-I and titin-II with isolated muscle, extramuscularly connected muscle, and epimuscularly connected muscle are compared to passive state titin with isolated muscle for fascicle section IV

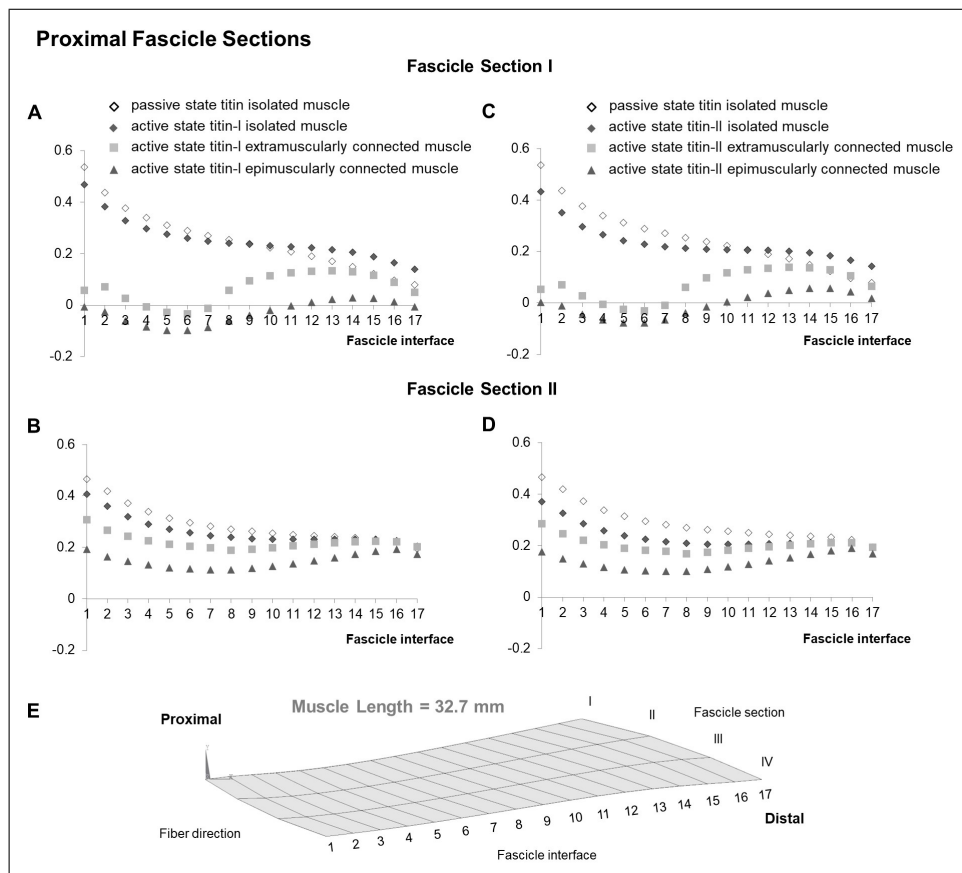


**Figure 4.4** Nodal fiber direction strains for proximal fascicle sections (I-II) at  $l_m = 32.7\text{mm}$  per fascicle interface. (A) (C) Active state titin-I and titin-II with isolated muscle, extramuscularly connected muscle, and epimuscularly connected muscle are compared to passive state titin with isolated muscle for fascicle section I. (B) (D) Active state titin-I and titin-II with isolated muscle, extramuscularly connected muscle, and epimuscularly connected muscle are compared to passive state titin with isolated muscle for fascicle section II

### Muscle fiber direction mean strains

Following details of effects of EMFT on nodal muscle fiber direction strains, Figs. 4.5 and 4.6 show muscle fiber direction mean strains and stresses at  $l_m = 32.7\text{mm}$  mm for active state titin-I and active state titin-II, respectively.

*Active state titin effect:* for isolated muscle, mean fiber direction strain curves of active state titin-I (Fig. 4.5A) and active state titin-II (Fig. 4.6A) are clearly localized below that of the passive state titin for all fascicle interfaces, which effect is referred to as the shorter sarcomere effect.

*EMFT manipulating effect:* the shorter sarcomere effect becomes an inconsistent and variable effect: for extramuscularly connected muscle, shorter sarcomere effect is enhanced for most fascicle interfaces (1 to 14, maximally by 16.8% and 17.4%, for fascicle interface 1 for active state titin-I and II, respectively). Conversely, it is diminished for the remaining fascicles (15 to 17, maximally by 2.0% and 2.7%, for fascicle interface 17 for active state titin-I and II, respectively). For epimuscularly connected muscle, SSE is further enhanced for most fascicle interfaces (1 to 13, maximally by 30.2% and 31.0%, for fascicle interface 1 for active state titin-I and II, respectively). SSE is also diminished for some fascicles (14 to 17, maximally by 10.3% and 14.0%, for fascicle interface 17 for active state titin-I and II, respectively), but even a longer sarcomere effect is shown for other fascicle interfaces (16-17 for active state titin-I and fascicle interface 17 for active state titin-II).

#### Muscle fiber direction mean total stress, contractile and titin stresses

*Active state titin effect:* for isolated muscle, muscle fiber direction mean total stress curves of active state titin-I (Fig.4.5B) and active state titin-II (Fig.4.6B) are above that of the passive state titin yielding an index for force production which is higher by 31.2% and 57.9%, respectively.

*EMFT manipulating effect:* for extramuscularly connected muscle, the index for force production increases by 34.8% and 60.1% and for epimuscularly connected muscle even further by 37.3% and 63.7% for active state titin-I and active state titin-II, respectively. This is ascribed to titin component to force production predominantly (Fig. 4.5D and Fig. 4.6D), but the contribution of the contractile component is also higher: for extramuscularly connected muscle, the contractile index for force production is higher by 8.5% (Fig. 4.5C) and 16.2% (Fig. 4.6C) for active state titin-I and active state titin-II, respectively, whereas for epimuscularly connected muscle, by 4.5% and 12.7%.

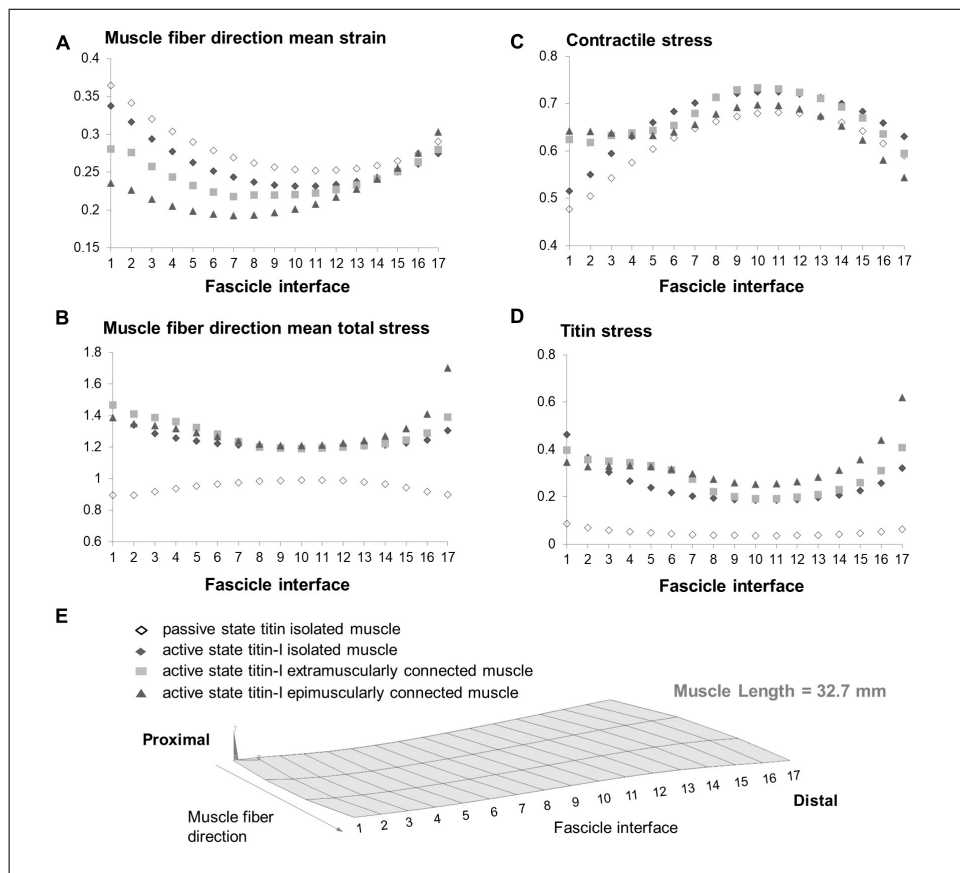


**Figure 4.5** Mean nodal fiber direction strain and stresses at  $l_m = 32.7\text{mm}$  per fascicle interface. Active state titin-I with isolated muscle, extramuscularly connected muscle, and epimuscularly connected muscle are compared to passive state titin with isolated muscle. (A) Mean fiber direction strain ( $\varepsilon_{22}$ ) across fascicle interfaces. (B) Mean nodal fiber direction contractile stress ( $\sigma_{22}^{\text{CONTR}}$ ) across fascicle interfaces. (C) Mean nodal fiber direction titin stress ( $\sigma_{22}^{\text{TITIN}}$ ) across fascicle interfaces. (D) Mean fiber direction total stress ( $\sigma_{22}$ ) across fascicle interfaces

### 4.3.2 Global effects of EMFT, manipulating functional effects of active state titin

Fig.4.7 shows muscle length-force characteristics for active state titin-I and active state titin-II.

*Active state titin effect:* for isolated muscle, compared to muscle forces of passive state titin, with increased muscle lengthening muscle forces increase by up to 37.5% (Fig. 4.7A) and 77.4% (Fig. 4.7B) for active state titin-I and active state titin-II, respectively. A shift of muscle's optimum length to a longer length (29.6 mm) is a remarkable effect of active state titin-II (Fig. 4.7B).

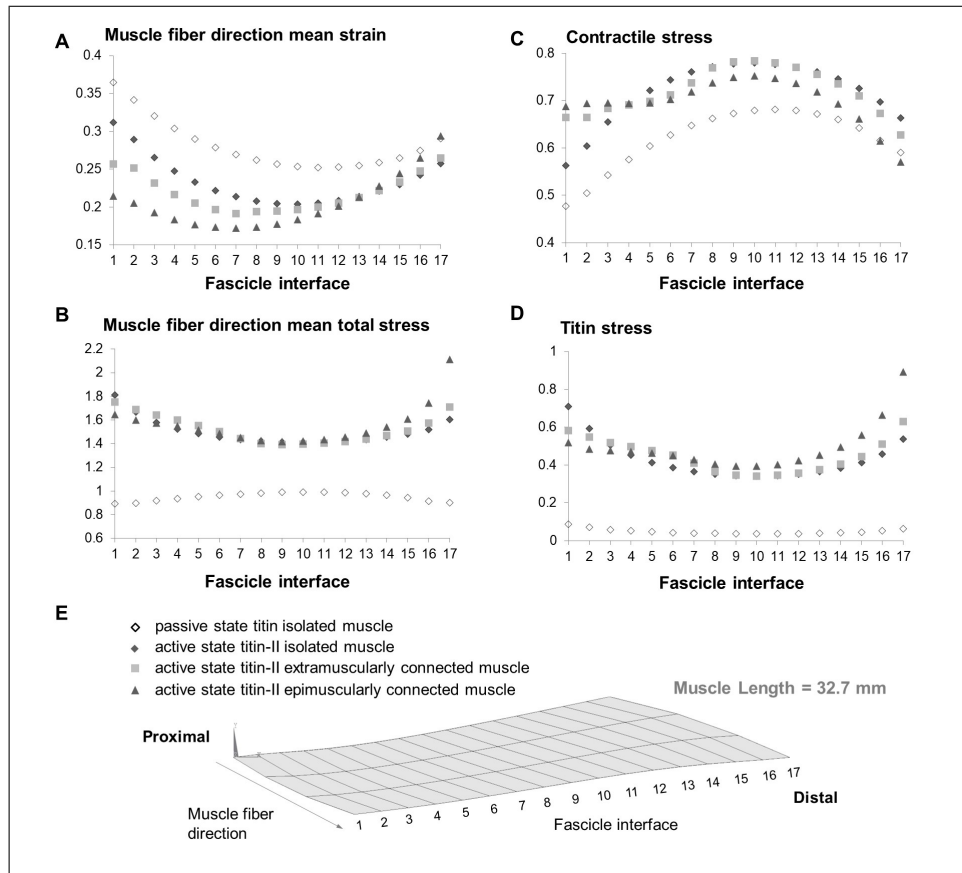


**Figure 4.6** Mean nodal fiber direction strain and stresses at  $l_m = 32.7\text{mm}$  per fascicle interface. Active state titin-II with isolated muscle, extramuscularly connected muscle, and epimuscularly connected muscle are compared to passive state titin with isolated muscle. (A) Mean fiber direction strain ( $\epsilon_{22}$ ) across fascicle interfaces. (B) Mean nodal fiber direction contractile stress ( $\sigma_{22\text{contr}}$ ) across fascicle interfaces. (C) Mean nodal fiber direction titin stress ( $\sigma_{22\text{titin}}$ ) across fascicle interfaces. (D) Mean fiber direction total stress ( $\sigma_{22}$ ) across fascicle interfaces

*EMFT manipulating effect:* Force differences are prominent and variable for all muscle lengths studied. At 28.7mm, for extramuscularly connected muscle, muscle force decreases by 4.4% and 2.3%, for active state titin-I and active state titin-II, respectively and for epimuscularly connected muscle, by 7.8% and 2.8%. At 32.7mm, for extramuscularly connected muscle, muscle force increases by 42.9% and 78.8% for active state titin-I and active state titin-II, respectively and for epimuscularly connected muscle, by 65.8% and 96.8%. A shift of muscle's optimum length to a different length is valid for both for extramuscularly connected muscle (to a longer length of 29.9 mm) and epimuscularly connected muscle (to a shorter muscle length of 28.7 mm) for active state titin-II (Fig. 4.7B).

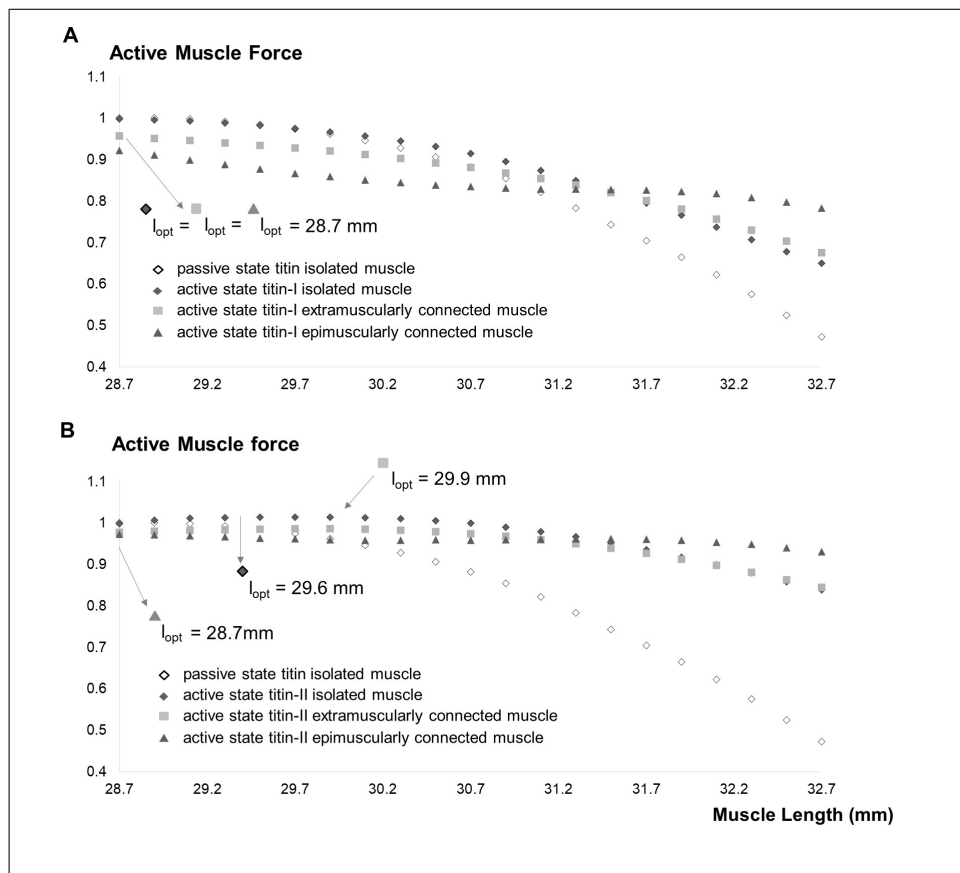


**Figure 4.7** The force-length characteristics of the modeled EDL muscles in the range of muscle lengths studied from initial length i.e.,  $l_m = 28.7\text{mm}$  to  $l_m = 32.7\text{mm}$ . (A) Active isometric muscle forces of different model cases are calculated as the difference between total and passive muscle forces. Forces of the passive state titin with isolated muscle and active state titin-I with isolated muscle, extramuscularly connected muscle, and epimuscularly connected muscle are shown. (B) Active isometric muscle forces of different model cases are calculated as the difference between total and passive muscle forces. Forces of the passive state titin with isolated muscle and active state titin-II with isolated muscle, extramuscularly connected muscle, and epimuscularly connected muscle are shown

## 4.4 Discussion

Our findings show that active state titin effects on muscular mechanics in isolated muscle do change in muscle with extra- and epimuscular connections. In isolated muscle the consistent characteristic effect of active state titin is the shorter sarcomere effect, which present itself as less lengthened sarcomeres than those encountered with passive state titin. However, the integrated muscles show locally major differences including even shortened sarcomeres in certain muscle parts and more or less pronounced shorter sarcomere effect in other parts. Therefore, our results confirmed our hypothesis.

Two calcium-dependent models to characterize the altered mechanical behavior of active state titin have been central to developing new muscle mechanics phenomena in the last years: (1) stiffening of titin PEVK region caused by the affinity of e-rich motifs in the PEVK segment (e.g., Labeit et al., 2003), and (2) titin N2A-actin interaction (e.g., Dutta et al., 2018) reducing titin's free-spring length to the PEVK segment and increasing overall titin stiffness[37],[130]. Both models account for an increase of sarcomere force in stretch induced conditions and enable new viewpoints in which titin is defined as the third myofilament[73],[56] or as a tunable spring[6] within the sarcomere. Incorporating these models in the whole muscle level, Cankaya et al. (2021) revealed their mechanism of effects on muscular mechanics, characterized by the shorter sarcomere effect. This was achieved with the LFMM model that incorporates an interconnected bi-domain modeling concept of muscle fibers and extracellular matrix. This concept enables mechanical interaction between these domains, such that the mechanical equilibrium determining local length changes of sarcomeres takes into account intramuscular myofascial loads exerted by the ECM on the muscle fibers. Active vs. passive state titin effects studied in that context in truly isolated muscle did show that active state titin can overcome myofascial loads and limit sarcomere lengthening[131].

On the other hand, for integrated muscle brought to long length, its mechanical interaction with surrounding muscular and connective tissue structures lead to loads to develop via stretching of the muscle's epimuscular connections. The net resultant of such epimuscular myofascial loads on the EDL muscle were previously made evident experimentally as muscle proximo-distal force differences[49],[78],[52],[53]. Such epimuscular myofascial loads exerted on the ECM also come into play and with intramuscular myofascial loads can manipulate sarcomere lengths. The extent of possible combined effects of such epi- and intramuscular myofascial loads were shown recently to be notable and different than those of solely intramuscular myofascial loads, to include strains opposing those elsewhere within the muscle that are determined by the globally imposed conditions[135]: (1) in passively lengthened integrated muscle, locally shortened regions and (2) in isometrically activated integrated muscle locally lengthened regions were shown. Note that, those model scenarios represent principles of experiments conducted in human muscle in vivo[105],[80]. The present study tack-

les the interaction of active state titin and epi- and intramuscular myofascial loads in integrated muscle context and shows this time that those loads can manipulate and overcome active state titin effects. Leading to heterogeneity of muscle fiber direction strains (implying nonuniformity of sarcomere length changes along fascicles), those myofascial loads enhance (by increased lengthening) or limit (by diminished lengthening) or even eliminate (by shortening) active state titin effects locally in different regions. Unlike in isolated muscle at long length in which all regions along muscle fibers lengthen, the latter represents a particularly interesting impact of epimuscular myofascial loads on active state titin effects because such shortened regions may even indicate disappeared differences between active and passive state titin.

Note that, mechanical interaction of integrated muscle with its surroundings consequently has remarkable functional effects reflected on muscle's length-force characteristics causing changes in amplitude of muscle forces and a shift in muscle's optimum length to different muscle lengths[136],[53]. Note however, the differential reflection of epimuscular myofascial loads on muscle function for active state titin-I and II. Force enhancement effect indicates an increased contribution of muscle to joint moment. This effect gets more pronounced in the presence of locally lengthened sarcomeres (i.e., shorter sarcomere effect counteracted by epimuscular myofascial loads) mainly for active state titin-II. However, with the presence of locally shortened regions of the muscle (i.e., shorter sarcomere effect further sustained by epimuscular myofascial loads) this effect vanishes for active state titin-I. Note that, for active state titin-II, owing to a reduction in titin's free-spring length, force enhancement remains, but gets decreased. On the other hand, a shift of muscle optimum length to a different muscle length alters muscle's contribution to joint range of movement. In isolated muscle, that effect was shown to be exclusive to active state titin-II[131]. In contrast, the current findings indicate that active state titin effects on muscle optimum length are dependent on epimuscular loads and thus can be sustained or eliminated based on muscle's interaction with its surrounding structures.

The presently modeled extramuscularly and epimuscularly connected muscles exemplify different scenarios of integrated muscle context with the former representing

a lesser epimuscular myofascial load-imposed scenario compared to the latter. Indeed, muscle is integrated with its surroundings via various tissues including collagen reinforced neurovascular tracts, intermuscular septa, and compartmental and general fascia[99],[102],[79] imposing loads[50],[137],[46],[54]. Such epimuscular loads present themselves during different body movements to varying extents[138],[46]. The present results showing differential functional effects of active state titin determined by epimuscular myofascial loads may be relevant clinically. Kinesio taping is used to improve muscle strength and joint range of motion in sportive performance, neuromusculoskeletal disorders and other injuries[139],[140]. It was shown that such externally imposed mechanical loading on the skin affects local strains in muscle and other tissues within and beyond the taped region[141], and also alters the contractile mechanics of the target muscle[142]. Those findings coupled with the present ones suggest that kinesio taping via epimuscular myofascial loads it develops in a broad tissue region may induce its functional effects by also manipulating active state titin's mechanics within the targeted muscle. In muscle spasticity e.g., in cerebral palsy, joint range of movement is compromised[143] suggesting a shift of  $l_{mo}$  to shorter muscle lengths and active state titin was shown to have the capacity to yield the opposite[131]. Therefore, we discussed earlier the possibility of a lack of active state titin mechanical influence to be responsible for the pathological spastic muscle function. However, measurements of active forces of human spastic gracilis[86], semitendinosus[87] and semimembranosus[77] muscles' directly as a function of knee joint angle during remedial surgery did not show low forces in extended knee positions, where the muscles are lengthened. This shows that sarcomeres of spastic muscles were not overstretched and hence do not imply that active state titin's shorter sarcomere effect was overcome by intermuscular mechanical interaction. Yet, in those experiments only the target muscles were activated. Co-activation intraoperatively of synergistic and antagonistic muscles and analyses in gait relevant joint positions did change spastic gracilis[88],[89] and semitendinosus[144] forces leading to significant shifts of peak force exertion to flexed knee positions. Therefore, in conditions involving more pronounced epimuscular myofascial loads spastic muscles' mechanics correlate with the pathological joint condition and this may be in part because of a diminished mechanical influence of active state titin, which requires further investigation. Note that, botulinum toxin type-A injections widely used in spastic-

ity management[145] can compromise intermuscular mechanical interaction[146] and remedial surgery techniques involve dissection of muscle's connections to surrounding structures[86], which can diminish epimuscular myofascial loads acting on the target muscle.

In conclusion, the present study showed that in the integrated muscle context, the role of active state titin as the third myofilament in muscular mechanics is manipulated by EMFT. This suggests that the classical two myofilament model, which remains incompetent for explaining several in situ muscle mechanics phenomena requires inclusion of active state titin and muscle fiber-to-ECM-to higher structural levels of myofascial connections to start characterizing in vivo muscle mechanics phenomena.

## 5. General Discussion

### 5.1 An alternative perspective for the Third Myofilament

Present thesis aims to introduce a new perspective to titin literature with comprehensive approach. In this regard, a series of analyses with finite element modeling are performed:

1. The work done in the second chapter had novel findings in terms of titin's mechanism of effect (shorter sarcomere effect) and functional effects (optimum muscle length shift to a longer length). Overall, the chapter emphasize the importance of this alternative approach in this regard.
2. Results of the third chapter showed that non-uniform strain distributions along the muscle fiber direction opposing the globally imposed effect are ascribed to epimuscular myofascial loads. These findings indicate of another component that can manipulate the mechanism of effect of titin, as SSE is an effect on sarcomere strain as well: That is, the titin becomes an active component and contributes to the skeletal muscle mechanics through affecting the sarcomere strain.
3. Findings of the work done in fourth chapter showed that active state titin effects on muscular mechanics in isolated muscle do change in muscle with extra- and epimuscular connections. Muscle in-vivo is not isolated; hence these results indicate that incorporating EMFT is a requirement in the analysis of active state titin's role in skeletal muscle mechanics.

### 5.2 An alternative perspective for the Three-Myofilament Model

Two myofilament model is insufficient, and titin is the third myofilament that contributing to force production. The widely adopted perspective to investigate titin in

this regard so far was to understanding titin's calcium dependent activation behaviors with an isolated focus on titin itself resulted with a progression on titin's calcium affinity and corresponding mechanical behaviors. However, the three-myofibril contractile model based on the findings of current approach where the contribution of non-force producing components to skeletal muscle mechanics are overlooked will lead to an insufficient model yet again. For the analysis of titin as an active component, present study assumed a comprehensive perspective where the contribution of non-force producing components in terms of intramuscular and epimuscular myofascial force transmission. In doing so, novel findings introduced to literature in terms of titin's mechanism of effect, its functionality, and its dependency to EMFT. These findings are the product of such alternative approach where titin's effect revealed due to the presence of myofascial force transmission and epimuscular loads. This implies an important aspect for defining a new contraction model: For the analysis of the components of the contractile machinery, contribution to force production and contribution to muscle mechanics should be assessed with alternative perspectives. Titin's calcium dependent mechanical behaviors belong to the former as these increases its stiffness, whereas its mechanism of effect SSE belongs to latter as this mechanism further translates its affect to other components as well as to muscle length force characteristics. These together comprehensively define titin's contribution as a component of third myofibril model.

In conclusion, aim of this thesis was to analyze titin's role in muscle contraction with an alternative perspective. In doing so, novel findings introduced to literature in terms of titin's mechanism of effect, its functionality, and its dependency to EMFT. Furthermore, the approach embraced in this thesis indicates that a new (comprehensive) perspective is required to fully understand the role of active titin in contractile machinery.

## APPENDIX A. APPENDIX A: LINKED FIBER MESH MATRIX MODEL

In the linked fiber-matrix mesh model (LFMM model), skeletal muscle is considered to consist of intracellular and extracellular matrix (ECM) domains. The trans sarcolemmal attachments (multimolecular structures including dystrophin, dystroglycan complex and laminin) are considered as elastic links between the two domains[59],[60]. Two user defined elements were developed in ANSYS 12.0: The ECM element represents the basal lamina, endomysium, perimysium and epimysium. The myofiber element models the muscle fibers. Both elements have eight nodes, linear interpolation functions and a large deformation analysis formulation. A 3D-local coordinate system representing the fiber, cross fiber and thickness directions is used. Separate meshes of ECM and myofiber elements occupying the same space are rigidly connected to single layers of aponeuroses and are linked elastically at intermediate nodes. In the LFMM model, one muscle element represents a segment of a bundle of muscle fibers, its connective tissues and the links between them(Figure(A.1a)).

### A.1 Isolated EDL muscle model

EDL muscle of the rat is a unipennate muscle with rather small pennation angles and minimal variation of the fiber direction within the muscle belly. The model geometry (Fig. A1b) is defined as the contour of a longitudinal slice at mid-muscle belly filled by three muscle elements in series and sixteen in parallel. Any collection of three muscle elements in series represents a muscle fascicle. Aponeurosis elements have identical mechanical properties, but increasing cross sectional area toward the tendon[61] is accounted for.

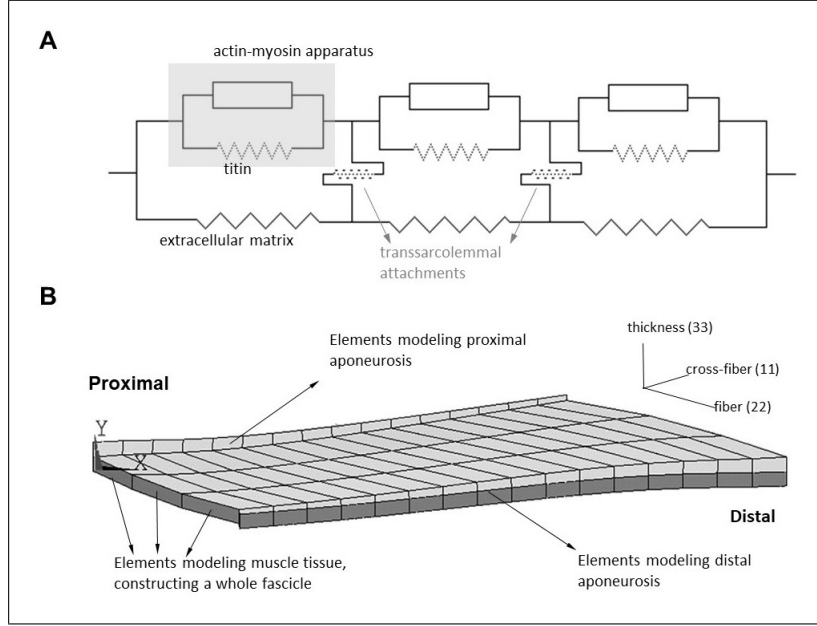


**Figure A.1** Finite element model of EDL muscle of the rat. (a) Two dimensional schematic representation of an arrangement of muscle elements. The intracellular domain, which is comprised of the contractile apparatus and titin is linked to the extracellular matrix domain elastically through transsarcolemmal attachments. (b) The model consists of three muscle elements in series and sixteen in parallel. Three muscle elements arranged in series construct a fascicle. A combination of nodes along one side of a fascicle is referred to as a fascicle interface. Each fascicle interface is indicated by a number from 1 to 17. The muscle elements located proximally and distally are connected to elements representing the muscles aponeuroses. A 3D local coordinate system representing the fiber, cross fiber (normal to the fiber direction), and thickness directions is used for the analysis and presentation of the model results[47]

### A.1.1 ECM element

The stress formulation is based on Second Piola-Kirchoff definition:

$$S = \frac{dW}{dL^G} \quad (\text{A.1})$$

A strain energy density function accounts for (1) non linear and anisotropic material properties(Huyghe et al., 1991) and (2) a penalty function to account for the constancy of muscle volume.

$$W = W_1 + W_2 \quad (\text{A.2})$$

$$W_1 = W_{ij}(\varepsilon_{ij}) \quad (\text{A.3})$$

where

$$W_{ij} = k(e^{a_{ij}\varepsilon_{ij}} - a_{ij}\varepsilon_{ij}) \quad \text{for } \varepsilon_{ij} > 0 \quad (\text{A.4})$$

or

$$W_{ij} = -W_{ij} |\varepsilon_{ij}| \quad \text{for } \varepsilon_{ij} < 0 \quad \text{and } i \neq j \quad (\text{A.5})$$

and  $\varepsilon_{ij}$  are the Green-Lagrange strains ( $dL^G$ ) in the local coordinates. The indices  $i$  and  $j = 1\dots 3$  represent the local cross fiber, fiber and thickness directions, respectively.  $a_{ij}$  and  $k$  are constants (Table A.1).

$$W_2 = \lambda_s(I_3 - 1)^2 + \lambda_f(I_3^{\text{avg}} - 1)^2 \quad (\text{A.6})$$

where,  $I_3$  is the third invariant of the right Cauchy-Green strain tensor, a measure for the local volume for each Gaussian integration point. If all the  $I_3$ 's are kept as unity, the element is considered as solid and the local volumes are conserved. If the weighted mean of all  $I_3$ 's per element,  $I_3^{\text{avg}}$  is kept as unity, the element is considered as a fluid. The penalty parameters  $\lambda_s$  and  $\lambda_f$  (Table 1), allow determining the emphasis given for each part (see Yucesoy and Huijing 2012 for further details). Resulting curves are given in figure A.2a.

### A.1.2 Myofiber element

Maximally activated muscle is studied and sarcomeres are assumed to have identical material properties. The total stress for the intracellular domain ( $\sigma_{22}$ ) is the sum of contractile ( $\sigma_{22\text{contr}}$ ) and titin ( $\sigma_{22\text{titin}}$ ) Cauchy stresses. At initial muscle length, in passive state, sarcomere lengths and material properties are assumed identical and the fiber direction strain ( $\sigma_{22}$ ) is zero. For  $\sigma_{22\text{contr}}$  experimental data of rat gastrocnemius medialis fiber bundles (Zuurbier et al., 1995) was fit with an exponential function and scaled such that at muscle optimum length ( $l_{\text{mo}}$ ),  $\sigma_{22}$  is zero and the

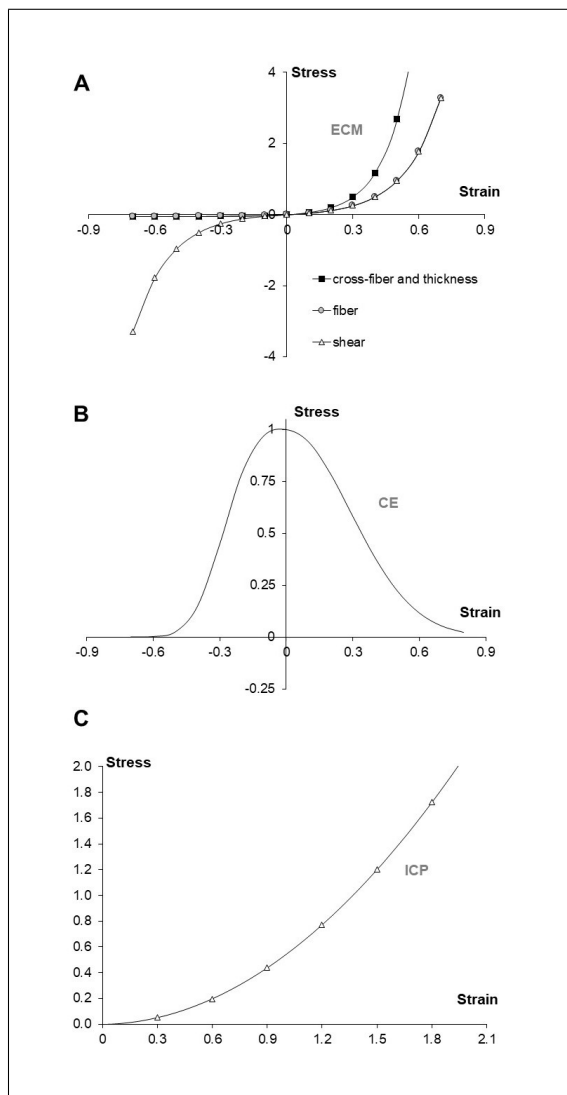


**Figure A.2** LFMM model concept and plots of constitutive equations defining the muscle modeled. (A) 2D schematic representation of an arrangement of muscle elements. The intracellular domain, which is composed of the active contractile elements (CEs) and intracellular passive cytoskeleton (ICP), is linked to the extracellular matrix (ECM) domain, elastically. (B) Extracellular matrix element stress-strain relations defined in fiber, cross-fiber, and thickness directions. (C) Myofiber element's active (contractile element) stress-strain relation defined in fiber direction. (D) Myofiber element's intracellular passive (titin) stress-strain relation defined in fiber direction.

maximal stress value is unity.

$$\sigma_{22\text{contr}}(\varepsilon_{22}) = b_3 e^{b_2 \varepsilon_{22}^2} \quad \text{for } \varepsilon_{22} > 0 \quad (\text{A.7})$$

or

$$\sigma_{22\text{contr}}(\varepsilon_{22}) = b_3 e^{b_1 \varepsilon_{22}^3} \quad \text{for } \varepsilon_{22} < 0 \quad (\text{A.8})$$

where  $b_1$ ,  $b_2$  and  $b_3$  are constants (Table A.1). Resulting curves are given in Figure A.2b. For  $\sigma_{22\text{titin}}$  in the passive state, experimental tension-sarcomere length data (Trombiti et al., 1995) for a single rabbit skeletal muscle fiber was fitted using a parabolic function and scaled to make it compatible to  $\sigma_{22\text{contr}}$ .

$$\sigma_{22\text{titin}}(\varepsilon_{22}) = t_1\varepsilon_{22}^2 + t_2\varepsilon_{22} + t_3 \quad (\text{A.9})$$

and

$$\sigma_{22\text{titin}}(\varepsilon_{22}) = 0 \quad \text{for} \quad \varepsilon_{22} = 0 \quad (\text{A.10})$$

where  $t_1$ ,  $t_2$  and  $t_3$  are constants (Table 1). Resulting curves are given in Figure A.2c.

### A.1.3 Linking elements

To represent the trans-sarcolemal attachments of the cytoskeleton and ECM, COMBIN39 (uniaxial 2 node spring element with linear stiffness) from ANSYS 12.0 was used.

### A.1.4 Aponeurosis element

HYPER58 (8 node, hyperelastic, 3D element, using the Mooney-Rivlin material law) from ANSYS 12.0 was used.

**Table A.1**  
Values and definitions of the model constants.

Constant	Value	Definition
$b_1$	30.0	Coefficient for the stress-strain relation of the contractile elements (EqnA.8)
$b_2$	-6.0	Coefficient for the stress-strain relation of the contractile elements (EqnA.7)
$b_3$	1	Coefficient for the stress-strain relation of the contractile elements (EqnA.7A.8)
$t_1$	0.522	Coefficient for the stress-strain relation of passive state titin (EqnA.9)
$t_2$	0.019	Coefficient for the stress-strain relation of passive state titin (EqnA.9)
$t_3$	-0.002	Coefficient for the stress-strain relation of passive state titin (EqnA.9)
$h_1$	3.204	Coefficient for the stress-strain relation of active state titin equations
$h_2$	1.811	Coefficient for the stress-strain relation of active state titin equations
$h_3$	0.207	Coefficient for the stress-strain relation of active state titin equations
$\varepsilon_{\text{shift}}$	0.11	Coefficient for the stress-strain relation of active state titin equations
$k$	0.05	Initial passive stiffness (EqnA.4)
$a_{11}$	8.0	Passive cross-fiber direction stiffness, $a_{11} = a_{33}$ (EqnA.4)
$a_{22}$	6.0	Passive fiber direction stiffness (EqnA.4)
$a_{12}$	6.0	Passive fiber-cross-fiber shear stiffness $a_{12} = a_{23} = a_{31}$ (EqnA.4)
$\lambda_s$	5.0	Weight factor in the penalty function for the solid volume (EqnA.6)
$\lambda_f$	20.0	Weight factor in the penalty function for the fluid volume (EqnA.6)

## REFERENCES

1. Huxley, H. E., "The Mechanism of Muscular Contraction," *Science*, Vol. 164, pp. 1356–1366, June 1969.
2. Huxley, H. E., "Fifty years of muscle and the sliding filament hypothesis," *European Journal of Biochemistry*, Vol. 271, pp. 1403–1415, Apr. 2004.
3. Huxley, A. F., and R. Niedergerke, "Measurement of the striations of isolated muscle fibres with the interference microscope," *The Journal of Physiology*, Vol. 144, pp. 403–425, Dec. 1958.
4. Gordon, A. M., A. F. Huxley, and F. J. Julian, "The variation in isometric tension with sarcomere length in vertebrate muscle fibres," *The Journal of Physiology*, Vol. 184, pp. 170–192, May 1966.
5. Herzog, W., "Skeletal muscle mechanics: questions, problems and possible solutions," *Journal of NeuroEngineering and Rehabilitation*, Vol. 14, p. 98, Dec. 2017.
6. Nishikawa, K., "Titin: A Tunable Spring in Active Muscle," *Physiology*, Vol. 35, pp. 209–217, May 2020.
7. Bagni, M. A., G. Cecchi, F. Colomo, and P. Garzella, "Development of stiffness precedes cross-bridge attachment during the early tension rise in single frog muscle fibres.," *The Journal of Physiology*, Vol. 481, pp. 273–278, Dec. 1994.
8. Herzog, W., E. J. Lee, and D. E. Rassier, "Residual force enhancement in skeletal muscle: Residual force enhancement in skeletal muscle," *The Journal of Physiology*, Vol. 574, pp. 635–642, Aug. 2006.
9. Herzog, W., and T. R. Leonard, "Force enhancement following stretching of skeletal muscle: a new mechanism," *The Journal of Experimental Biology*, Vol. 205, pp. 1275–1283, May 2002.
10. Abbott, B. C., and X. M. Aubert, "The force exerted by active striated muscle during and after change of length," *The Journal of Physiology*, Vol. 117, pp. 77–86, May 1952.
11. Maruyama, K., R. Natori, and Y. Nonomura, "New elastic protein from muscle," *Nature*, Vol. 262, pp. 58–60, July 1976.
12. Bang, M.-L., T. Centner, F. Fornoff, A. J. Geach, M. Gotthardt, M. McNabb, C. C. Witt, D. Labeit, C. C. Gregorio, H. Granzier, and S. Labeit, "The Complete Gene Sequence of Titin, Expression of an Unusual 700-kDa Titin Isoform, and Its Interaction With Obscurin Identify a Novel Z-Line to I-Band Linking System," *Circulation Research*, Vol. 89, pp. 1065–1072, Nov. 2001.
13. Tskhovrebova, L., and J. Trinick, "Roles of Titin in the Structure and Elasticity of the Sarcomere," *Journal of Biomedicine and Biotechnology*, Vol. 2010, pp. 1–7, 2010.
14. Meyer, L. C., and N. T. Wright, "Structure of giant muscle proteins," *Frontiers in Physiology*, Vol. 4, 2013.
15. Linke, W. A., "Stretching molecular springs: elasticity of titin filaments in vertebrate striated muscle," *Histology and Histopathology*, pp. 799–811, July 2000.

16. Labeit, S., and B. Kolmerer, "Titins: Giant Proteins in Charge of Muscle Ultrastructure and Elasticity," *Science*, Vol. 270, pp. 293–296, Oct. 1995.
17. Linke, W. A., and N. Hamdani, "Gigantic Business: Titin Properties and Function Through Thick and Thin," *Circulation Research*, Vol. 114, pp. 1052–1068, Mar. 2014.
18. Lindstedt, S., and K. Nishikawa, "Huxleys' Missing Filament: Form and Function of Titin in Vertebrate Striated Muscle," *Annual Review of Physiology*, Vol. 79, pp. 145–166, Feb. 2017.
19. Wang, K., and R. Ramirez-Mitchell, "A network of transverse and longitudinal intermediate filaments is associated with sarcomeres of adult vertebrate skeletal muscle.," *The Journal of Cell Biology*, Vol. 96, pp. 562–570, Feb. 1983.
20. Trombitis, K., J.-P. Jin, and H. Granzier, "The Mechanically Active Domain of Titin in Cardiac Muscle," *Circulation Research*, Vol. 77, pp. 856–861, Oct. 1995.
21. Lee, E.-J., J. Peng, M. Radke, M. Gotthardt, and H. L. Granzier, "Calcium sensitivity and the Frank-Starling mechanism of the heart are increased in titin N2B region-deficient mice," *Journal of Molecular and Cellular Cardiology*, Vol. 49, pp. 449–458, Sept. 2010.
22. Pfuhl, M., and M. Gautel, "Structure, interactions and function of the N-terminus of cardiac myosin binding protein C (MyBP-C): who does what, with what, and to whom?," *Journal of Muscle Research and Cell Motility*, Vol. 33, pp. 83–94, May 2012.
23. Linke, W. A., M. Ivemeyer, P. Mundel, M. R. Stockmeier, and B. Kolmerer, "Nature of PEVK-titin elasticity in skeletal muscle," *Proceedings of the National Academy of Sciences*, Vol. 95, pp. 8052–8057, July 1998.
24. Horowitz, R., and R. J. Podolsky, "The positional stability of thick filaments in activated skeletal muscle depends on sarcomere length: evidence for the role of titin filaments.," *Journal of Cell Biology*, Vol. 105, pp. 2217–2223, Nov. 1987.
25. Horowitz, R., E. S. Kempner, M. E. Bisher, and R. J. Podolsky, "A physiological role for titin and nebulin in skeletal muscle," *Nature*, Vol. 323, pp. 160–164, Sept. 1986.
26. Lee, E.-J., V. Joumaa, and W. Herzog, "New insights into the passive force enhancement in skeletal muscles," *Journal of Biomechanics*, Vol. 40, pp. 719–727, Jan. 2007.
27. Bagni, M. A., G. Cecchi, B. Colombini, and F. Colomo, "A Non-Cross-Bridge Stiffness in Activated Frog Muscle Fibers," *Biophysical Journal*, Vol. 82, pp. 3118–3127, June 2002.
28. Leonard, T. R., and W. Herzog, "Regulation of muscle force in the absence of actin-myosin-based cross-bridge interaction," *American Journal of Physiology-Cell Physiology*, Vol. 299, pp. C14–C20, July 2010.
29. Linke, W. A., "Titin Gene and Protein Functions in Passive and Active Muscle," *Annual Review of Physiology*, Vol. 80, pp. 389–411, Feb. 2018.
30. Minajeva, A., C. Neagoe, M. Kulke, and W. A. Linke, "Titin-based contribution to shortening velocity of rabbit skeletal myofibrils," *The Journal of Physiology*, Vol. 540, pp. 177–188, Apr. 2002.
31. Linke, W., M. Stockmeier, M. Ivemeyer, H. Hossler, and P. Mundel, "Characterizing titin's I-band Ig domain region as an entropic spring," *Journal of Cell Science*, Vol. 111, pp. 1567–1574, June 1998.

32. Kellermayer, M. S., and H. L. Granzier, "Calcium-dependent inhibition of in vitro thin-filament motility by native titin," *FEBS Letters*, Vol. 380, pp. 281–286, Feb. 1996.
33. Rivas-Pardo, J., E. Eckels, I. Popa, P. Kosuri, W. Linke, and J. Fernández, "Work Done by Titin Protein Folding Assists Muscle Contraction," *Cell Reports*, Vol. 14, pp. 1339–1347, Feb. 2016.
34. Tatsumi, R., K. Maeda, A. Hattori, and K. Takahashi, "Calcium binding to an elastic portion of connectin/titin filaments," *Journal of Muscle Research and Cell Motility*, Vol. 22, no. 2, pp. 149–162, 2001.
35. Labeit, D., K. Watanabe, C. Witt, H. Fujita, Y. Wu, S. Lahmers, T. Funck, S. Labeit, and H. Granzier, "Calcium-dependent molecular spring elements in the giant protein titin," *Proceedings of the National Academy of Sciences*, Vol. 100, pp. 13716–13721, Nov. 2003.
36. Joumaa, V., D. E. Rassier, T. R. Leonard, and W. Herzog, "The origin of passive force enhancement in skeletal muscle," *American Journal of Physiology-Cell Physiology*, Vol. 294, pp. C74–C78, Jan. 2008.
37. Nishikawa, K. C., J. A. Monroy, T. E. Uyeno, S. H. Yeo, D. K. Pai, and S. L. Lindstedt, "Is titin a 'winding filament'? A new twist on muscle contraction," *Proceedings of the Royal Society B: Biological Sciences*, Vol. 279, pp. 981–990, Mar. 2012.
38. Dutta, S., C. Tsiros, S. L. Sundar, H. Athar, J. Moore, B. Nelson, M. J. Gage, and K. Nishikawa, "Calcium increases titin N2A binding to F-actin and regulated thin filaments," *Scientific Reports*, Vol. 8, p. 14575, Dec. 2018.
39. Monroy, J. A., K. L. Powers, C. M. Pace, T. Uyeno, and K. C. Nishikawa, "Effects of activation on the elastic properties of intact soleus muscles with a deletion in titin," *The Journal of Experimental Biology*, p. jeb.139717, Dec. 2016.
40. Tahir, U., J. A. Monroy, N. A. Rice, and K. C. Nishikawa, "Effects of a titin mutation on force enhancement and force depression in mouse soleus muscles," *The Journal of Experimental Biology*, Vol. 223, p. jeb197038, Jan. 2020.
41. Hessel, A. L., V. Joumaa, S. Eck, W. Herzog, and K. C. Nishikawa, "Optimal length, calcium sensitivity and twitch characteristics of skeletal muscles from *mdm* mice with a deletion in N2A titin," *The Journal of Experimental Biology*, Vol. 222, p. jeb200840, June 2019.
42. Powers, K., K. Nishikawa, V. Joumaa, and W. Herzog, "Decreased force enhancement in skeletal muscle sarcomeres with a deletion in titin," *Journal of Experimental Biology*, p. jeb.132027, Jan. 2016.
43. Powers, K., G. Schappacher-Tilp, A. Jinha, T. Leonard, K. Nishikawa, and W. Herzog, "Titin force is enhanced in actively stretched skeletal muscle," *Journal of Experimental Biology*, Vol. 217, pp. 3629–3636, Oct. 2014.
44. Gillies, A. R., and R. L. Lieber, "Structure and function of the skeletal muscle extracellular matrix: Skeletal Muscle ECM," *Muscle & Nerve*, Vol. 44, pp. 318–331, Sept. 2011.
45. Purslow, P. P., "The Structure and Role of Intramuscular Connective Tissue in Muscle Function," *Frontiers in Physiology*, Vol. 11, p. 495, May 2020.

46. Wilke, J., R. Schleip, C. A. Yucesoy, and W. Banzer, "Not merely a protective packing organ? A review of fascia and its force transmission capacity," *Journal of Applied Physiology*, Vol. 124, pp. 234–244, Jan. 2018.
47. Yucesoy, C. A., B. H. F. J. M. Koopman, H. J. Grootenboer, and P. A. Huijing, "Finite element modeling of aponeurotomy: altered intramuscular myofascial force transmission yields complex sarcomere length distributions determining acute effects," *Biomechanics and Modeling in Mechanobiology*, Vol. 6, pp. 227–243, June 2007.
48. Maas, H., "Significance of epimuscular myofascial force transmission under passive muscle conditions," *Journal of Applied Physiology*, Vol. 126, pp. 1465–1473, May 2019.
49. Huijing, P., and G. Baan, "Myofascial Force Transmission Causes Interaction between Adjacent Muscles and Connective Tissue: Effects of Blunt Dissection and Compartmental Fasciotomy on Length Force Characteristics of Rat Extensor Digitorum Longus Muscle," *Archives of Physiology and Biochemistry*, Vol. 109, pp. 97–109, Jan. 2001.
50. Huijing, P. A., and G. C. Baan, "Myofascial Force Transmission via Extramuscular Pathways Occurs between Antagonistic Muscles," *Cells Tissues Organs*, Vol. 188, no. 4, pp. 400–414, 2008.
51. Maas, H., G. C. Baan, and P. A. Huijing, "Intermuscular interaction via myofascial force transmission: effects of tibialis anterior and extensor hallucis longus length on force transmission from rat extensor digitorum longus muscle," *Journal of Biomechanics*, Vol. 34, pp. 927–940, July 2001.
52. Yucesoy, C., B. Koopman, G. Baan, H. Grootenboer, and P. Huijing, "Extramuscular Myofascial Force Transmission: Experiments and Finite Element Modeling," *Archives of Physiology and Biochemistry*, Vol. 111, pp. 377–388, Jan. 2003.
53. Yucesoy, C. A., B. H. Koopman, G. C. Baan, H. J. Grootenboer, and P. A. Huijing, "Effects of inter- and extramuscular myofascial force transmission on adjacent synergistic muscles: assessment by experiments and finite-element modeling," *Journal of Biomechanics*, Vol. 36, pp. 1797–1811, Dec. 2003.
54. Yucesoy, C. A., "Epimuscular Myofascial Force Transmission Implies Novel Principles for Muscular Mechanics," *Exercise and Sport Sciences Reviews*, Vol. 38, pp. 128–134, July 2010.
55. Linke, W. A., and H. Granzier, "A Spring Tale: New Facts on Titin Elasticity," *Biophysical Journal*, Vol. 75, pp. 2613–2614, Dec. 1998.
56. Herzog, W., "The multiple roles of titin in muscle contraction and force production," *Biophysical Reviews*, Vol. 10, pp. 1187–1199, Aug. 2018.
57. Neagoe, C., C. A. Opitz, I. Makarenko, and W. A. Linke, "Gigantic variety: expression patterns of titin isoforms in striated muscles and consequences for myofibrillar passive stiffness," *Journal of Muscle Research and Cell Motility*, Vol. 24, no. 2/3, pp. 175–189, 2003.
58. Garvey, S. M., C. Rajan, A. P. Lerner, W. N. Frankel, and G. A. Cox, "The Muscular Dystrophy with Myositis (mdm) Mouse Mutation Disrupts a Skeletal Muscle-Specific Domain of Titin," *Genomics*, Vol. 79, pp. 146–149, Feb. 2002.

59. Yucesoy, C. A., B. H. Koopman, P. A. Huijing, and H. J. Grootenboer, "Three-dimensional finite element modeling of skeletal muscle using a two-domain approach: linked fiber-matrix mesh model," *Journal of Biomechanics*, Vol. 35, pp. 1253–1262, Sept. 2002.
60. Yucesoy, C. A., and P. A. Huijing, "SPECIFICALLY TAILORED USE OF THE FINITE ELEMENT METHOD TO STUDY MUSCULAR MECHANICS WITHIN THE CONTEXT OF FASCIAL INTEGRITY: THE LINKED FIBER-MATRIX MESH MODEL," *International Journal for Multiscale Computational Engineering*, Vol. 10, no. 2, pp. 155–170, 2012.
61. Zuurbier, C. J., A. J. Everard, P. van der Wees, and P. A. Huijing, "Length-force characteristics of the aponeurosis in the passive and active muscle condition and in the isolated condition," *Journal of Biomechanics*, Vol. 27, pp. 445–453, Apr. 1994.
62. Yucesoy, C. A., and P. A. Huijing, "Substantial effects of epimuscular myofascial force transmission on muscular mechanics have major implications on spastic muscle and remedial surgery," *Journal of Electromyography and Kinesiology*, Vol. 17, pp. 664–679, Dec. 2007.
63. Nagy, A., L. Grama, T. Huber, P. Bianco, K. Trombitás, H. Granzier, and M. Kellermayer, "Hierarchical Extensibility in the PEVK Domain of Skeletal-Muscle Titin," *Biophysical Journal*, Vol. 89, pp. 329–336, July 2005.
64. Ma, K., and K. Wang, "Malleable conformation of the elastic PEVK segment of titin: non-co-operative interconversion of polyproline II helix, b-turn and unordered structures," *Biochemical Journal*, Vol. 374, pp. 687–695, Sept. 2003.
65. Huber, T., L. Grama, C. Hetényi, G. Schay, L. Földesi, B. Penke, and M. Kellermayer, "Conformational Dynamics of Titin PEVK Explored with FRET Spectroscopy," *Biophysical Journal*, Vol. 103, pp. 1480–1489, Oct. 2012.
66. Linke, W., M. Ivemeyer, S. Labeit, H. Hinssen, J. Riegler, and M. Gautel, "Actin-titin interaction in cardiac myofibrils: probing a physiological role," *Biophysical Journal*, Vol. 73, pp. 905–919, Aug. 1997.
67. Yamasaki, R., M. Berri, Y. Wu, K. Trombitás, M. McNabb, M. Kellermayer, C. Witt, D. Labeit, S. Labeit, M. Greaser, and H. Granzier, "Titin-Actin Interaction in Mouse Myocardium: Passive Tension Modulation and Its Regulation by Calcium/S100A1," *Biophysical Journal*, Vol. 81, pp. 2297–2313, Oct. 2001.
68. Fukushima, H., C. S. Chung, and H. Granzier, "Titin-Isoform Dependence of Titin-Actin Interaction and Its Regulation by S100A1/ Ca<sup>2+</sup> in Skinned Myocardium," *Journal of Biomedicine and Biotechnology*, Vol. 2010, pp. 1–9, 2010.
69. Linke, W. A., and J. Fernandez, "Cardiac titin: Molecular basis of elasticity and cellular contribution to elastic and viscous stiffness components in myocardium," *Journal of Muscle Research and Cell Motility*, Vol. 23, no. 5/6, pp. 483–497, 2002.
70. Astier, C., F. Raynaud, M.-C. Lebart, C. Roustan, and Y. Benyamin, "Binding of a native titin fragment to actin is regulated by PIP<sub>2</sub>," *FEBS Letters*, Vol. 429, pp. 95–98, June 1998.
71. Niederlander, N., F. Raynaud, C. Astier, and P. Chaussepied, "Regulation of the actin-myosin interaction by titin," *European Journal of Biochemistry*, Vol. 271, pp. 4572–4581, Nov. 2004.

72. Nagy, A., P. Cacciafesta, L. Grama, A. Kengyel, A. M̃;lñ;si-Csizmadia, and M. S. Z. Kellermayer, "Differential actin binding along the PEVK domain of skeletal muscle titin," *Journal of Cell Science*, Vol. 117, pp. 5781–5789, Nov. 2004.
73. Schappacher-Tilp, G., T. Leonard, G. Desch, and W. Herzog, "A Novel Three-Filament Model of Force Generation in Eccentric Contraction of Skeletal Muscles," *PLOS ONE*, Vol. 10, p. e0117634, Mar. 2015.
74. Tomalka, A., C. Rode, J. Schumacher, and T. Siebert, "The active force-length relationship is invisible during extensive eccentric contractions in skinned skeletal muscle fibres," *Proceedings of the Royal Society B: Biological Sciences*, Vol. 284, p. 20162497, May 2017.
75. Watanabe, D., C. R. Lamboley, and G. D. Lamb, "Effects of S-glutathionylation on the passive force length relationship in skeletal muscle fibres of rats and humans," *Journal of Muscle Research and Cell Motility*, Nov. 2019.
76. Willems, M. E. T., and P. A. Huijing, "Heterogeneity of mean sarcomere length in different fibres: effects on length range of active force production in rat muscle," *European Journal of Applied Physiology and Occupational Physiology*, Vol. 68, pp. 489–496, Nov. 1994.
77. Yucesoy, C. A., Y. Temelli, and F. Ates, "Intra-operatively measured spastic semimembranosus forces of children with cerebral palsy," *Journal of Electromyography and Kinesiology*, Vol. 36, pp. 49–55, Oct. 2017.
78. Maas, H., G. C. Baan, P. A. Huijing, C. A. Yucesoy, B. H. F. J. M. Koopman, and H. J. Grootenboer, "The Relative Position of EDL Muscle Affects the Length of Sarcomeres Within Muscle Fibers: Experimental Results and Finite-Element Modeling," *Journal of Biomechanical Engineering*, Vol. 125, pp. 745–753, Oct. 2003.
79. Yucesoy, C. A., H. Maas, B. H. Koopman, H. J. Grootenboer, and P. A. Huijing, "Mechanisms causing effects of muscle position on proximo-distal muscle force differences in extra-muscular myofascial force transmission," *Medical Engineering & Physics*, Vol. 28, pp. 214–226, Apr. 2006.
80. Pamuk, U., A. Karakuzu, C. Ozturk, B. Acar, and C. A. Yucesoy, "Combined magnetic resonance and diffusion tensor imaging analyses provide a powerful tool for in vivo assessment of deformation along human muscle fibers," *Journal of the Mechanical Behavior of Biomedical Materials*, Vol. 63, pp. 207–219, Oct. 2016.
81. Karakuzu, A., U. Pamuk, C. Ozturk, B. Acar, and C. A. Yucesoy, "Magnetic resonance and diffusion tensor imaging analyses indicate heterogeneous strains along human medial gastrocnemius fascicles caused by submaximal plantar-flexion activity," *Journal of Biomechanics*, Vol. 57, pp. 69–78, May 2017.
82. Heidlauf, T., T. Klotz, C. Rode, T. Siebert, and O. Rohrlé, "A continuum-mechanical skeletal muscle model including actin-titin interaction predicts stable contractions on the descending limb of the force-length relation," *PLOS Computational Biology*, Vol. 13, p. e1005773, Oct. 2017.
83. Raiteri, B. J., "Aponeurosis behaviour during muscular contraction: A narrative review," *European Journal of Sport Science*, Vol. 18, pp. 1128–1138, Sept. 2018.
84. Lieber, R. L., and J. Fridlén, "Spasticity causes a fundamental rearrangement of muscle-joint interaction," *Muscle & Nerve*, Vol. 25, pp. 265–270, Feb. 2002.

85. Smith, L. R., K. S. Lee, S. R. Ward, H. G. Chambers, and R. L. Lieber, "Hamstring contractures in children with spastic cerebral palsy result from a stiffer extracellular matrix and increased *in vivo* sarcomere length: Passive mechanical properties of muscle contracture," *The Journal of Physiology*, Vol. 589, pp. 2625–2639, May 2011.
86. Ates, F., Y. Temelli, and C. A. Yucesoy, "Human spastic Gracilis muscle isometric forces measured intraoperatively as a function of knee angle show no abnormal muscular mechanics," *Clinical Biomechanics*, Vol. 28, pp. 48–54, Jan. 2013.
87. Ates, F., Y. Temelli, and C. A. Yucesoy, "The mechanics of activated semitendinosus are not representative of the pathological knee joint condition of children with cerebral palsy," *Journal of Electromyography and Kinesiology*, Vol. 28, pp. 130–136, June 2016.
88. Ates, F., and C. A. Yucesoy, "Effects of botulinum toxin type A on non-injected bi-articular muscle include a narrower length range of force exertion and increased passive force: Complex Effects of BTX-A," *Muscle & Nerve*, Vol. 49, pp. 866–878, June 2014.
89. Kaya, C. S., F. Bilgili, N. E. Akalan, Y. Temelli, F. Ates, and C. A. Yucesoy, "Intraoperative experiments combined with gait analyses indicate that active state rather than passive dominates the spastic gracilis muscle's joint movement limiting effect in cerebral palsy," *Clinical Biomechanics*, Vol. 68, pp. 151–157, Aug. 2019.
90. Kaya, C. S., F. Bilgili, N. E. Akalan, and C. A. Yucesoy, "Intraoperative testing of passive and active state mechanics of spastic semitendinosus in conditions involving intermuscular mechanical interactions and gait relevant joint positions," *Journal of Biomechanics*, Vol. 103, p. 109755, Apr. 2020.
91. Huijing, P. A., "Muscle as a collagen fiber reinforced composite: a review of force transmission in muscle and whole limb," *Journal of Biomechanics*, Vol. 32, pp. 329–345, Apr. 1999.
92. Rowe, R. W., "ULTRASTRUCTURE OF THE Z LINE OF SKELETAL MUSCLE FIBERS," *Journal of Cell Biology*, Vol. 51, pp. 674–685, Dec. 1971.
93. Pardo, J. V., J. D. Siliciano, and S. W. Craig, "A vinculin-containing cortical lattice in skeletal muscle: transverse lattice elements ("costameres") mark sites of attachment between myofibrils and sarcolemma.," *Proceedings of the National Academy of Sciences*, Vol. 80, pp. 1008–1012, Feb. 1983.
94. Danowski, B. A., K. Imanaka-Yoshida, J. M. Sanger, and J. W. Sanger, "Costameres are sites of force transmission to the substratum in adult rat cardiomyocytes.," *Journal of Cell Biology*, Vol. 118, pp. 1411–1420, Sept. 1992.
95. Berthier, C., and S. Blaineau, "Supramolecular organization of the subsarcolemmal cytoskeleton of adult skeletal muscle fibers. A review," *Biology of the Cell*, Vol. 89, pp. 413–434, Oct. 1997.
96. Trotter, J. A., and P. P. Purslow, "Functional morphology of the endomysium in series fibered muscles," *Journal of Morphology*, Vol. 212, pp. 109–122, May 1992.
97. Street, S. F., "Lateral transmission of tension in frog myofibers: A myofibrillar network and transverse cytoskeletal connections are possible transmitters," *Journal of Cellular Physiology*, Vol. 114, pp. 346–364, Mar. 1983.

98. Huijing, P. A., and G. C. Baan, "Extramuscular myofascial force transmission within the rat anterior tibial compartment: proximo-distal differences in muscle force: Extramuscular myofascial force transmission," *Acta Physiologica Scandinavica*, Vol. 173, pp. 297–311, Nov. 2001.
99. Huijing, P. A., H. Maas, and G. C. Baan, "Compartmental fasciotomy and isolating a muscle from neighboring muscles interfere with myofascial force transmission within the rat anterior crural compartment," *Journal of Morphology*, Vol. 256, pp. 306–321, June 2003.
100. Stecco, A., S. Masiero, V. Macchi, C. Stecco, A. Porzionato, and R. De Caro, "The pectoral fascia: Anatomical and histological study," *Journal of Bodywork and Movement Therapies*, Vol. 13, pp. 255–261, July 2009.
101. Willard, F. H., A. Vleeming, M. D. Schuenke, L. Danneels, and R. Schleip, "The thoracolumbar fascia: anatomy, function and clinical considerations: The thoracolumbar fascia," *Journal of Anatomy*, Vol. 221, pp. 507–536, Dec. 2012.
102. Wilke, J., T. Engeroff, F. NÄ¼rnberger, L. Vogt, and W. Banzer, "Anatomical study of the morphological continuity between iliotibial tract and the fibularis longus fascia," *Surgical and Radiologic Anatomy*, Vol. 38, pp. 349–352, Apr. 2016.
103. Huijing, P. A., "Epimuscular myofascial force transmission: A historical review and implications for new research. International society of biomechanics Muybridge award lecture, Taipei, 2007," *Journal of Biomechanics*, Vol. 42, pp. 9–21, Jan. 2009.
104. Ates, F., Y. Temelli, and C. A. Yucesoy, "Effects of antagonistic and synergistic muscles' co-activation on mechanics of activated spastic semitendinosus in children with cerebral palsy," *Human Movement Science*, Vol. 57, pp. 103–110, Feb. 2018.
105. Huijing, P. A., A. Yaman, C. Ozturk, and C. A. Yucesoy, "Effects of knee joint angle on global and local strains within human triceps surae muscle: MRI analysis indicating in vivo myofascial force transmission between synergistic muscles," *Surgical and Radiologic Anatomy*, Vol. 33, pp. 869–879, Dec. 2011.
106. Toupin, R. A., "Saint-Venant's Principle," *Archive for Rational Mechanics and Analysis*, Vol. 18, pp. 83–96, Jan. 1965.
107. van Eijden, T. M. G. J., and M. C. Raadsheer, "Heterogeneity of fiber and sarcomere length in the human masseter muscle," *The Anatomical Record*, Vol. 232, pp. 78–84, Jan. 1992.
108. Moo, E. K., R. Fortuna, S. C. Sibole, Z. Abusara, and W. Herzog, "In vivo Sarcomere Lengths and Sarcomere Elongations Are Not Uniform across an Intact Muscle," *Frontiers in Physiology*, Vol. 7, May 2016.
109. Lichtwark, G. A., D. J. Farris, X. Chen, P. W. Hodges, and S. L. Delp, "Microendoscopy reveals positive correlation in multiscale length changes and variable sarcomere lengths across different regions of human muscle," *Journal of Applied Physiology*, Vol. 125, pp. 1812–1820, Dec. 2018.
110. Heemskerk, A. M., T. K. Sinha, K. J. Wilson, Z. Ding, and B. M. Damon, "Repeatability of DTI-based skeletal muscle fiber tracking: REPEATABILITY OF DTI-BASED FIBER TRACKING," *NMR in Biomedicine*, Vol. 23, pp. 294–303, Apr. 2010.

111. Froeling, M., A. J. Nederveen, D. F. Heijtel, A. Lataster, C. Bos, K. Nicolay, M. Maas, M. R. Drost, and G. J. Strijkers, "Diffusion-tensor MRI reveals the complex muscle architecture of the human forearm," *Journal of Magnetic Resonance Imaging*, Vol. 36, pp. 237–248, July 2012.
112. Sinha, U., S. Sinha, J. A. Hodgson, and R. V. Edgerton, "Human soleus muscle architecture at different ankle joint angles from magnetic resonance diffusion tensor imaging," *Journal of Applied Physiology*, Vol. 110, pp. 807–819, Mar. 2011.
113. Felton, S. M., T. A. Gaige, T. Benner, R. Wang, T. G. Reese, V. J. Wedeen, and R. J. Gilbert, "Associating the mesoscale fiber organization of the tongue with local strain rate during swallowing," *Journal of Biomechanics*, Vol. 41, no. 8, pp. 1782–1789, 2008.
114. Asakawa, D., G. Pappas, S. Blemker, J. Drace, and S. Delp, "Cine Phase-Contrast Magnetic Resonance Imaging As a Tool for Quantification of Skeletal Muscle Motion," *Seminars in Musculoskeletal Radiology*, Vol. 7, no. 4, pp. 287–296, 2003.
115. Tian, M., R. D. Herbert, P. Hoang, S. C. Gandevia, and L. E. Bilston, "Myofascial force transmission between the human soleus and gastrocnemius muscles during passive knee motion," *Journal of Applied Physiology*, Vol. 113, pp. 517–523, Aug. 2012.
116. Ettema, G. J., and P. A. Huijing, "Properties of the tendinous structures and series elastic component of EDL muscle-tendon complex of the rat," *Journal of Biomechanics*, Vol. 22, pp. 1209–1215, Jan. 1989.
117. Huijing, P., G. C. Baan, and G. T. Rebel, "Non-myotendinous force transmission in rat extensor digitorum longus muscle," *Journal of Experimental Biology*, Vol. 201, pp. 683–691, Mar. 1998.
118. Huijing, P., S. Nieberg, E. v.d. Veen, and G. Ettema, "A Comparison of Rat Extensor digitorum longus and Gastrocnemius medialis Muscle Architecture and Length-Force Characteristics," *Cells Tissues Organs*, Vol. 149, no. 2, pp. 111–120, 1994.
119. Jaspers, R., R. Brunner, G. Baan, and P. Huijing, "Acute effects of intramuscular aponeurotomy and tenotomy on multitendoned rat EDL: Indications for local adaptation of intramuscular connective tissue," *The Anatomical Record*, Vol. 266, pp. 123–135, Feb. 2002.
120. Huijing, P. A., and G. C. Baan, "Myofascial force transmission: muscle relative position and length determine agonist and synergist muscle force," *Journal of Applied Physiology*, Vol. 94, pp. 1092–1107, Mar. 2003.
121. Yucesoy, C. A., G. C. Baan, B. H. F. J. M. Koopman, H. J. Grootenboer, and P. A. Huijing, "Pre-Strained Epimuscular Connections Cause Muscular Myofascial Force Transmission to Affect Properties of Synergistic EHL and EDL Muscles of the Rat," *Journal of Biomechanical Engineering*, Vol. 127, pp. 819–828, Oct. 2005.
122. Maas, H., G. C. Baan, and P. A. Huijing, "Muscle force is determined also by muscle relative position: isolated effects," *Journal of Biomechanics*, Vol. 37, pp. 99–110, Jan. 2004.
123. Bernabei, M., J. H. van Dieën, G. C. Baan, and H. Maas, "Significant mechanical interactions at physiological lengths and relative positions of rat plantar flexors," *Journal of Applied Physiology*, Vol. 118, pp. 427–436, Feb. 2015.

124. Turkoglu, A. N., P. A. Huijing, and C. A. Yucesoy, "Mechanical principles of effects of botulinum toxin on muscle length-force characteristics: An assessment by finite element modeling," *Journal of Biomechanics*, Vol. 47, pp. 1565–1571, May 2014.
125. Yaraskavitch, M., T. Leonard, and W. Herzog, "Botox produces functional weakness in non-injected muscles adjacent to the target muscle," *Journal of Biomechanics*, Vol. 41, pp. 897–902, Jan. 2008.
126. Yucesoy, C. A., and F. Ates, "BTX-A has notable effects contradicting some treatment aims in the rat triceps surae compartment, which are not confined to the muscles injected," *Journal of Biomechanics*, Vol. 66, pp. 78–85, Jan. 2018.
127. Turkoglu, A. N., and C. A. Yucesoy, "Simulation of effects of botulinum toxin on muscular mechanics in time course of treatment based on adverse extracellular matrix adaptations," *Journal of Biomechanics*, Vol. 49, pp. 1192–1198, May 2016.
128. Kaya, C. S., Y. Temelli, F. Ates, and C. A. Yucesoy, "Effects of inter-synergistic mechanical interactions on the mechanical behaviour of activated spastic semitendinosus muscle of patients with cerebral palsy," *Journal of the Mechanical Behavior of Biomedical Materials*, Vol. 77, pp. 78–84, Jan. 2018.
129. Bagni, M. A., B. Colombini, F. Colomo, R. B. Palmi, and G. Cecchi, "Non Cross-Bridge Stiffness in Skeletal Muscle Fibres at Rest and During Activity," in *Sliding Filament Mechanism in Muscle Contraction* (Sugi, H., ed.), Vol. 565, pp. 141–155, Boston, MA: Springer US, 2005. Series Title: Advances in Experimental Medicine and Biology.
130. Nishikawa, K., "Eccentric contraction: unraveling mechanisms of force enhancement and energy conservation," *The Journal of Experimental Biology*, Vol. 219, pp. 189–196, Jan. 2016.
131. Cankaya, A. O., U. Pamuk, and C. A. Yucesoy, "The effects of an activation-dependent increase in titin stiffness on whole muscle properties using finite element modeling," *Journal of Biomechanics*, Vol. 116, p. 110197, Feb. 2021.
132. Adstrum, S., G. Hedley, R. Schleip, C. Stecco, and C. A. Yucesoy, "Defining the fascial system," *Journal of Bodywork and Movement Therapies*, Vol. 21, pp. 173–177, Jan. 2017.
133. Stecco, C., S. Adstrum, G. Hedley, R. Schleip, and C. A. Yucesoy, "Update on fascial nomenclature," *Journal of Bodywork and Movement Therapies*, Vol. 22, p. 354, Apr. 2018.
134. Schleip, R., G. Hedley, and C. A. Yucesoy, "Fascial nomenclature: Update on related consensus process," *Clinical Anatomy*, Vol. 32, pp. 929–933, Oct. 2019.
135. Pamuk, U., A. O. Cankaya, and C. A. Yucesoy, "Principles of the Mechanism for Epimuscular Myofascial Loads Leading to Non-uniform Strain Distributions Along Muscle Fiber Direction: Finite Element Modeling," *Frontiers in Physiology*, Vol. 11, p. 789, July 2020.
136. Ates, F., Y. Temelli, and C. A. Yucesoy, "Intraoperative experiments show relevance of inter-antagonistic mechanical interaction for spastic muscle's contribution to joint movement disorder," *Clinical Biomechanics*, Vol. 29, pp. 943–949, Sept. 2014.
137. Maas, H., W. Noort, H. A. Smilde, J. A. Vincent, P. Nardelli, and T. C. Cope, "Detection of epimuscular myofascial forces by Golgi tendon organs," *Experimental Brain Research*, Vol. 240, pp. 147–158, Jan. 2022.

138. Krause, F., J. Wilke, L. Vogt, and W. Banzer, "Intermuscular force transmission along myofascial chains: a systematic review," *Journal of Anatomy*, Vol. 228, pp. 910–918, June 2016.
139. Bassett, K. T., S. A. Lingman, and R. F. Ellis, "The use and treatment efficacy of kinaesthetic taping for musculoskeletal conditions: a systematic review," *New Zealand Journal of Physiotherapy*, Vol. 38, pp. 56+, July 2010. 56.
140. Harput, G., H. Guney, U. Toprak, F. Colakoglu, and G. Baltaci, "Acute effects of scapular Kinesio Taping on shoulder rotator strength, ROM and acromiohumeral distance in asymptomatic overhead athletes," *The Journal of Sports Medicine and Physical Fitness*, Vol. 57, Sept. 2017.
141. Pamuk, U., and C. A. Yucesoy, "MRI analyses show that kinesio taping affects much more than just the targeted superficial tissues and causes heterogeneous deformations within the whole limb," *Journal of Biomechanics*, Vol. 48, pp. 4262–4270, Dec. 2015.
142. Yildiz, S., U. Pamuk, G. Baltaci, and C. A. Yucesoy, "Effects of Kinesio Taping on Muscle Contractile Properties: Assessment Using Tensiomyography," *Journal of Sport Rehabilitation*, Vol. 31, pp. 263–270, Mar. 2022.
143. Bell, K. J., S. Ounpuu, P. A. DeLuca, and M. J. Romness, "Natural progression of gait in children with cerebral palsy," *Journal of Pediatric Orthopedics*, Vol. 22, pp. 677–682, Oct. 2002.
144. Kaya, C. S., E. O. Yilmaz, Z. D. Akdeniz-Dogan, and C. A. Yucesoy, "Long-Term Effects With Potential Clinical Importance of Botulinum Toxin Type-A on Mechanics of Muscles Exposed," *Frontiers in Bioengineering and Biotechnology*, Vol. 8, p. 738, June 2020.
145. Love, S. C., J. P. Valentine, E. M. Blair, C. J. Price, J. H. Cole, and P. J. Chauvel, "The effect of botulinum toxin type A on the functional ability of the child with spastic hemiplegia a randomized controlled trial," *European Journal of Neurology*, Vol. 8, pp. 50–58, Nov. 2001.
146. Yucesoy, C. A., A. N. Turkoglu, S. Umur, and F. Ates, "Intact muscle compartment exposed to botulinum toxin type a shows compromised intermuscular mechanical interaction: BTX-A Compromises Mechanics," *Muscle & Nerve*, Vol. 51, pp. 106–116, Jan. 2015.